PEOPLE'S DEMOCRATIC REPUBLIC OF ALGERIA
MINISTRY OF HIGHER EDUCATION AND SCIENTIFIC RESEARCH

DR. TAHAR MOULAY UNIVERSITY – SAIDA

Faculty of Science

Department of Chemistry

A Thesis

In Fulfillment of the Requirements
of Masters of Chemistry
(Inorganic Chemistry)

Submitted by

Ismail Mokaddem
July 17, 2019

Theme

Experimental and theoretical Study of complexation properties of metals with bidentate ligands

Jury Members

President	Mrs. Asmaa Mostefai	Professor	Saïda University
Examiner	Mr. Abdelkrim Guendouzi	MCA	Saïda University
Examiner	Mr. H. Ouici Boumedien	MCA	Saïda University
Supervisor	Mr. Houari Brahim	MCA	Saïda University

Fall 2019

ACKNOWLEDGEMENT

I would first like to thank my master thesis advisor **Dr**. **Houari Brahim**, for all his help and guidance that he has given me over the past four months. You have set an example of excellence as a researcher, mentor, instructor, and role model.

I would like to thank my sub-advisor and my co-worker **A.Sehmi, Ph.D.** for guiding and supporting me over this work period.

I would like to thank my thesis committee members President **Professor Asmaa Mostefai**.

I also want to thank **Dr. Abdelkrim Guendouzi** and **Dr. H. Ouici Boumedien** for all of their guidance through this process; your discussion, ideas, and feedback have been absolutely invaluable.

I would especially like to thank my amazing family for the love, support, and constant encouragement I have gotten over the years. In particular, I would like to thank my parents, my brother, my two amazing sisters and my brilliant uncle, teacher and friend **Bouazza Ahmed**. You are the salt of the earth, and I undoubtedly could not have done this without you.

I would also like to thank the two families **MOKADDEM** and **BOUAZZA**, and I am happy to be a member between them.

I would like to thank some special and amazing people in my life, **Sofiane Litim, Abdessamed Abdelli, Abdelghani Sehmi, LeaAnn Mcdonald, Moahmmed Daoudi, Oussama zaoui** and **Elhacene Bouziane**.

Last but not least, deepest thanks go to all people who took part in making this thesis real.

Ismail,

DEDICATION

This study is wholeheartedly dedicated to my beloved parents, who have been my source of inspiration and gave me strength when I thought of giving up, who continually provide their moral, spiritual, emotional, and financial support.

To my brothers, sisters, relatives, mentor, friends, and classmates who shared their words of advice and encouragement

And lastly, I dedicated this work to the Arabic and Islamic nation, to **Abdelhamid Ben Badis, Mohamed Bachir El Ibrahimi, Malcolm X, Saddam Hussein, Mahmoud Mohamed Chaker, Ahmed Deedat, Farid al-Ansari, Ali Ezzat Begovic** and all the greatest people of our nation.

List of Figures

List of Tables

Acronyms

DCM	Dichloromethane
DMF	Dimethylformamide
DFT	Density functional theory
TDDFT	Time-dependent density-functional theory
PCM	Polarizable continuum model
NMR	Necluar magnetic resoanace
IR	Infrared
UV	Ultraviolet
FMO	Frontier molecular orbital
HOMO	Highest occupied molecular orbital
LUMO	Lowest unoccupied molecular orbital
LMCT	Lignad to metal charge transfer
LLCT	Ligand to ligand charge transfer
MLCT	Metal to ligand charge transfer
LB	Ligand
Str	Stretching
Rock	Rocking
Bend	Bending

“It is hard to fail, but it is worse never to have tried to succeed.”

Theodore Roosevelt

Contents

Chapter II

METHODOLOGY

Chapter III

Results and Discussion

Introduction

Introduction

In the last decade, transition metal complexes with quinazolione ligands have attracted much attention and have been studied extensively in both experimental and theoretical areas[1.2]. The quinazoline ring system along with many alkaloids is widely recognized in inorganic syntheses and medicinal applications, for example, in HIV reverse transcriptase inhibitors. Some of them or their metal are used as biological models in understanding of biomolecules and biological processes. Such compounds have become the center of creating new drugs, some with highly active compounds have been commercialized such as fungicide fuquinconazole, anti-cancer drug, antihypertensive pyrazosin, etc. Some transition metal complexes with quinazoline analogs have been investigated in coordination chemistry and biological chemistry, although much remains to be understood. Nickel(II) complexes with oxime-type ligands have been widely investigated in coordination and biological chemistry, but cleavage of tow C-N bonds of shiff bases have not been observed in reaction with metal salts, and there is more interest about complexes in general, this is due to their rich applications in many fields: as catalyst supports [3.4], in the fields of organic lightemitting diodes OLED [5.6], as antimicrobial agents in biological activities [7], and as candidates for anticancer agents [8.9].

LAN-QIN CHAI and coworkers, have been synthesized an unexpected mononuclear Ni(II) complex[Ni(L^2)$_2$]-CH3OH(HL^2=1-(2-{[(E)-3,5-dichloro-2-hydroxybenzylidene]amino} phenyl)ethanoneoxime) via complexation of Ni(II) acetate tetrahydrate with HL^1. HL^1 and its corresponding Ni(II) complex were characterized byIR, ^{1}H-NMR spectra, HRMS, as well as by elemental analysis, UV–vis, and emission spectroscopy.The crystal structure of the complex has been determined by single-crystal X-ray diffraction. Eachcomplex links two other molecules into an infinite 1-D chain via intermolecular hydrogen bonds.Moreover, the electrochemical properties of the nickel complex were studied by cyclic

voltammetry.Superoxide dismutase-like activities of HL^1 and Ni(II) complex were also investigated.[10]

In the present work (theoretical), we studied theoretically the geometric structures, frontier molecular orbital (FMO) character, energy gaps and UV spectra of $[Ni(L^2)_2]$ by density functional theory (DFT) and time-dependent DFT (TD-DFT) calculations. The theoretical results are compared with experimental data. Also regarding to the experimental work, this part includes, the synthesis of a Schiff base ligand, N, N'-ethylenebis(2-benzoylpyridine imine) denoted as LB and their corresponding metalcomplexes like Cu(II) and Co(II) and they were characterized by ^{1}H NMR, ^{13}C NMR (LB) and IR (Cu(II)), (Co(II)).

Chapter I

Coordination Compounds
And Spectroscopy

I.1 Coordination Compounds:

Coordination compounds are composed of a metal atom or ion and one or more ligands (atoms, ions, or molecules) that donate electrons to the metal, this definition includes compounds with metal–carbon bonds, or organometallic compounds.

Coordination compound comes from the coordinate covalent bond, which historically was considered to form by donation of a pair of electrons from one atom to another. In coordination compounds, the donors are usually the ligands, and the acceptors are the metals. Coordination compounds are examples of acid–base adducts, frequently called complexes or, if charged, complex ions.[11]

I.1.1 Transition Elements:

I.1.1.a Definition and proprieties:

The transition elements may be strictly defined as those that, as elements, have partly filled *d* or *f* shells. Here we shall adopt a slightly broader definition and include elements that have partly filled *d* or *f* shells in any of their commonly occurring oxidation states. This means that we treat the coinage metals, Cu, Ag and Au, as transition metals, since Cu(II) has a $3d^9$ configura-

tion, Ag(II) a $4d^9$ configuration and Au(III) a $5d^8$ configuration. From a purely chemical point of view it is also appropriate to consider these elements as transition elements since their chemical behavior is, on the whole, quite similar to that of other transition elements. With the above broad definition in mind, one finds that there are at present some 56 transition elements, counting the heaviest elements through the one of atomic number 104, Clearly, the majority of all known elements are transition elements. All these transition elements have certain general properties in common:

- They are all metals.
- They are practically all hard, strong, high-melting, high-boiling metals that conduct heat and electricity well. In short, they are "typical" metals of the sort we meet in ordinary circumstances.
- They form alloys with one another and with other metallic elements.
- 4. Many of them are sufficiently electropositive to dissolve in mineral acids, although a few are “noble” that is, they have such low electrode potentials that they are unaffected by simple acids.

- With very few exceptions, they exhibit variable valence, and their ions and compounds are colored in one if not all oxidation states.
- Because of partially filled shells they form at least some paramagnetic compounds.[12]

I.1.2 Ligands:

In an inorganic coordination entity, the atoms or groups joined to the central atom.[13] Also In coordination chemistry, a ligand is an ion or molecule that binds to a central metal atom to form a coordination complex. The bonding with the metal generally involves formal donation of one or more of the ligand's electron pairs. The nature of metal–ligand bonding can range from covalent to ionic. Furthermore, the metal–ligand bond order can range from one to three. Ligands are viewed as Lewis bases, although rare cases are known to involve Lewis acidic "ligands".[14.15]

I.1.3 The Covalent Bond Classification Method:

In essence, the CBC method seeks to classify a molecule according to the nature of the ligands around the central element of interest. The method is based on the notion that there are three basic types of interaction by which a ligand may bond to a metal center and the ligand is classified according to the nature and number of these interactions.

The three basic types of interaction are represented by the symbols L, X, and Z, which correspond respectively to 2-electron, 1-electron and 0-electron *neutral* ligands and are clearly differentiated according to a molecular orbital representation of the bonding.

I.1.3.a L ligands:

The simplest case is that of molecules that coordinate with the metal via a free pair carried by one of their atoms Fig.1 . These molecules are L ligands, the metal-ligand bond being ensured by the two electrons provided by the ligand. Examples include NR3 amines and PR3 phosphines, which have a free pair on the nitrogen or phosphorus atom, the water molecule or any ether (OR2) that can coordinate with the metal through one of the two free pairs of the oxygen atom. Carbon monoxide is also a type L ligand via the free pair carried by the carbon atom.

Fig.1 Ligands type L (σ−complexes).

There are other cases in which the two electrons provided characterize a binding between two atoms of the L ligand, and no longer a free pair. It can be a binding π, as in the ethylene molecule, or, more curiously, a σ binding, as for the dihydrogen molecule Fig.2.

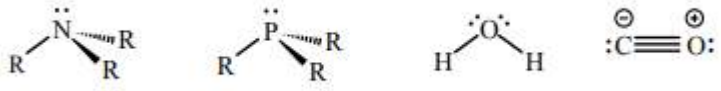

Fig.2 Ligands type L.

I.1.3.b X ligands:

These ligands bring only one electron into the coordination sphere of the metal. In the neutral state, the X ligands are radicals and the metal-ligand bond is by the single electron of the ligand and by an electron of the metal. Hydrogen (H) is a ligand X, as well as halogens (F, Cl, Br, I), alkyl radicals (CR3), amido (NR2), alkoxyl (OR), cyano (CN), Fig.3

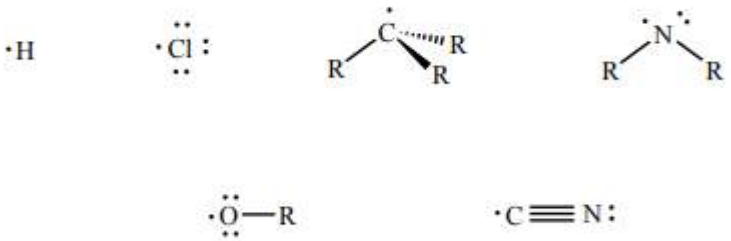

Fig.3 Ligands type X.

I.1.4 Other Types of ligands:

I.1.4.a Monodentate ligand:

This will coordinate to only site of a metal ion. In other words, it can donate only one pair of electrons to the metal ion.

I.1.4.b Bidentate ligand:

This will occupy two sites of a metal ion. That is, it can attach itself to two positions of a metal ion.

I.1.4.c Polydentate ligand:

These ligands occupy many sites of the same metal ion.

I.2 Schiff base:

A Schiff base (named after Hugo Schiff) is a compound with the general structure $R_2C=NR'$ ($R' \neq H$). They can be considered a sub-class of imines, being either secondary ketimines or secondary aldimines depending on their structure. The term is often synonymous with azomethine which refers specifically to secondary aldimines (i.e. R-CH=NR' where $R' \neq H$). A number of special naming systems exist for these compounds. For instance a Schiff base derived from an aniline, where R^3 is a phenyl or a substituted phenyl, can be called an anil, while bis-compounds are often referred to as salen-type compounds.

The term Schiff base is normally applied to these compounds when they are being used as ligands to form coordination complexes with metal ions. Such complexes occur naturally, for instance in Corrin, but the majority of Schiff bases are artificial and are used to form many important catalysts, such as Jacobsen's catalyst.

I.3 Structures of Metal Complexes:

The coordination numbers of metal ions in metal complexes can range from 2 to at least 9. In general, the differences in energy between different arrangements of ligands are greatest for complexes with low coordination numbers and decrease as the coordination number increases. Usually only one or two structures are possible for complexes with low coordination numbers, whereas several different energetically equivalent structures are possible for complexes with high coordination numbers ($n > 6$). The following presents the most commonly encountered structures for coordination numbers 2–9. Many of these structures should be familiar to you

from our discussion of the valence-shell electron-pair repulsion (VSEPR) model because they correspond to the lowest-energy arrangements of n electron pairs around a central atom.

I.3.1 Coordination Numbers:

The coordination number of a specified atom in a chemical species is the number of other atoms directly linked to that specified atom.

Note: I have chosen the two famous coordination numbers 4 and 6 featured below.

I.3.1.a Coordination Number 4:

Two common structures are observed for four-coordinate metal complexes: tetrahedral and square planar. The tetrahedral structure is observed for all four-coordinate complexes of non-transition metals, such as $[BeF_4]^{2-}$, and d^{10} ions, such as $[ZnCl_4]^{2-}$. It is also found for four-coordinate complexes of the first-row transition metals, especially those with halide ligands (e.g., $[FeCl_4]^-$ and $[FeCl_4]^{2-}$). In contrast, square planar structures are routinely observed for four-coordinate complexes of second- and third-row transition metals with d^8 electron configurations, such as Rh^+ and Pd^{2+}, and they are also encountered in some complexes of Ni^{2+} and Cu^{2+}.

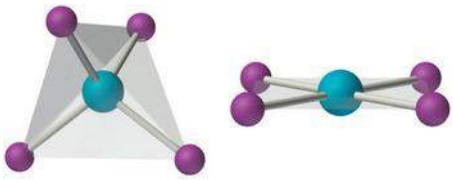

Fig.1 Tetrahedral and square planar ML_4

I.3.3 Coordination Number 6:

This coordination number is by far the most common. The six ligands are almost always at the vertices of an octahedron or a distorted octahedron. The only other six-coordinate structure is the trigonal prism, which is very uncommon in simple metal complexes.[17]

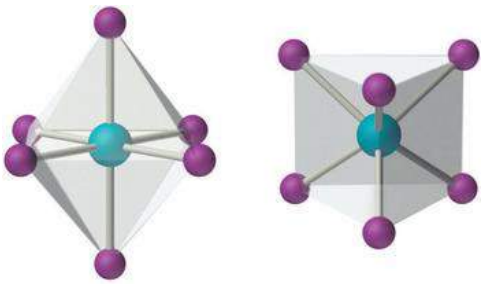

Fig.2 Octahedral and Trigonal prismatic ML_6

I.3.4 Octahedral complexes:

There are huge numbers of complexes with nominally octahedral geometry, where in this context the nominal structure 'ML_6' is taken to mean a central metal atom surrounded by six ligands, not all of which are necessarily the same.[18]

I.3.5 Tetrahedral complexes:

A tetrahedral complex where the centrally located metal ion has four ligands arranged as the hydrogen atoms in methane or a square planar geometry with the four ligands at the corner.[19]

I.4 Oxidation Number:

The oxidation number, or oxidation state, of an atom is the charge that would exist on the atom if the bonding were completely ionic. This oxidation number is an indicator of the degree of oxidation (loss of electrons) of an atom in a chemical compound. Conceptually, the oxidation state, which may be positive, negative or zero, is the hypothetical charge that an atom would have if all bonds to atoms of different elements were 100% ionic, with no covalent component. Oxidation number are typically represented by small integers.[20]

I.5 Electronic Structure:

There are two widely used models of the electronic structure of d-metal complexes. One ('crystal-field theory') emerged from an analysis of the spectra of d-metal ions in solids; the other ('ligand-field theory') arose from an application of molecular orbital theory. Crystalfield theory is more primitive, and strictly speaking it applies only to ions in crystals; however, it can be used to capture the essence of the electronic structure of complexes in a straightforward

manner. Ligand-field theory builds on crystal-field theory: it gives a more complete description of the electronic structure of complexes and accounts for a wider range of properties.

I.6 Crystal Field Theory:

In crystal-field theory, a ligand lone pair is modelled as a point negative charge (or as the partial negative charge of an electric dipole) that repels electrons in the d orbitals of the central metal ion. The theory concentrates on the resulting splitting of the d orbitals into groups with different energies, and uses that splitting to rationalize and correlate the optical spectra, thermodynamic stability, and magnetic properties of complexes.[21]

I.7 Ligand Field Theory:

Ligand field theory (LFT) describes the bonding, orbital arrangement, and other characteristics of coordination complexes.[22.23.24] It represents an application of molecular orbital theory to transition metal complexes. A transition metal ion has nine valence atomic orbitals - consisting of five *n*d, three (*n*+1)p, and one (*n*+1)s orbitals. These orbitals are of appropriate energy to form bonding interaction with ligands. The LFT analysis is highly dependent on the geometry of the complex, but most explanations begin by describing octahedral complexes, where six ligands coordinate to the metal.[25]

I.8 Molecular Orbitals:

In chemistry, a molecular orbital (MO) is a mathematical function describing the wave-like behavior of an electron in a molecule. This function can be used to calculate chemical and physical properties such as the probability of finding an electron in any specific region. The term orbital was introduced by Robert S. Mulliken in 1932 as an abbreviation for one-electron orbital wave function. At an elementary level, it is used to describe the region of space in which the function has a significant amplitude. Molecular orbitals are usually constructed by combining atomic orbitals or hybrid orbitals from each atom of the molecule, or other molecular orbitals from groups of atoms. They can be quantitatively calculated using the Hartree–Fock or self-consistent field (SCF) methods.[26]

A molecular orbital (MO) can be used to represent the regions in a molecule where an electron occupying that orbital is likely to be found. Molecular orbitals are obtained from the combination of atomic orbitals, which predict the location of an electron in an atom. A molecular orbital can specify the electron configuration of a molecule: the spatial distribution and energy of one (or one pair of) electron(s). Most commonly a MO is represented as a linear combination of atomic orbitals (the LCAO-MO method), especially in qualitative or very

approximate usage. They are invaluable in providing a simple model of bonding in molecules, understood through molecular orbital theory. Most present-day methods in computational chemistry begin by calculating the MOs of the system. A molecular orbital describes the behavior of one electron in the electric field generated by the nuclei and some average distribution of the other electrons. In the case of two electrons occupying the same orbital, the Pauli principle demands that they have opposite spin. Necessarily this is an approximation, and highly accurate descriptions of the molecular electronic wave function do not have orbitals (see configuration interaction).

Molecular orbitals are, in general, delocalized throughout the entire molecule. Moreover, if the molecule has symmetry elements, its nondegenerate molecular orbitals are either symmetric or antisymmetric with respect to any of these symmetries. In other words, application of a symmetry operation S (e.g., a reflection, rotation, or inversion) to molecular orbital ψ results in the molecular orbital being unchanged or reversing its mathematical sign: $S\psi = \pm\psi$. In planar molecules, for example, molecular orbitals are either symmetric (sigma) or antisymmetric (pi) with respect to reflection in the molecular plane. If molecules with degenerate orbital energies are also considered, a more general statement that molecular orbitals form bases for the irreducible representations of the molecule's symmetry group holds.[27]

I.8.1 Formation of molecular orbitals:

Molecular orbitals arise from allowed interactions between atomic orbitals, which are allowed if the symmetries (determined from group theory) of the atomic orbitals are compatible with each other. Efficiency of atomic orbital interactions is determined from the overlap (a measure of how well two orbitals constructively interact with one another) between two atomic orbitals, which is significant if the atomic orbitals are close in energy. Finally, the number of molecular orbitals formed must be equal to the number of atomic orbitals in the atoms being combined to form the molecule.[28]

I.8.2 Molecular orbital theory:

The molecular orbital theory (MOT) is widely used by chemists. It includes both the covalent and ionic character of chemical bonds, although it does not specifically mention either. MOT treats the electron distribution in molecules in very much the same way that modern atomic theory treats the electron distribution in atoms. First, the positions of atomic nuclei are determined. Then orbitals around nuclei are defined; these molecular orbitals (MO's) locate the

region in space in which an electron in a given orbital is most likely to be found. Rather than being localized around a single atom, these MO's extend over part or all of the molecule.[29]

I.9 The classification of bonds:

I.9.1 Ionic Bonds:

Ionic bonding is the complete transfer of valence electron(s) between atoms. It is a type of chemical bond that generates two oppositely charged ions. In ionic bonds, the metal loses electrons to become a positively charged cation, whereas the nonmetal accepts those electrons to become a negatively charged anion. Ionic bonds require an electron donor, often a metal, and an electron acceptor, a nonmetal.

Ionic bonding is observed because metals have few electrons in their outer-most orbitals. By losing those electrons, these metals can achieve noble gas configuration and satisfy the octet rule. Similarly, nonmetals that have close to 8 electrons in their valence shells tend to readily accept electrons to achieve noble gas configuration. In ionic bonding, more than 1 electron can be donated or received to satisfy the octet rule. The charges on the anion and cation correspond to the number of electrons donated or received. In ionic bonds, the net charge of the compound must be zero.

I.9.2 Covalent Bonds :

Covalent bonding is the sharing of electrons between atoms. This type of bonding occurs between two atoms of the same element or of elements close to each other in the periodic table. This bonding occurs primarily between nonmetals; however, it can also be observed between nonmetals and metals.

If atoms have similar electronegativities (the same affinity for electrons), covalent bonds are most likely to occur. Because both atoms have the same affinity for electrons and neither has a tendency to donate them, they share electrons in order to achieve octet configuration and become more stable. In addition, the ionization energy of the atom is too large and the electron affinity of the atom is too small for ionic bonding to occur. For example: carbon does not form ionic bonds because it has 4 valence electrons, half of an octet. To form ionic bonds, Carbon molecules must either gain or lose 4 electrons. This is highly unfavorable; therefore, carbon molecules share their 4 valence electrons through single, double, and triple bonds so that each atom can achieve noble gas configurations. Covalent bonds include interactions of the sigma

and pi orbitals; therefore, covalent bonds lead to formation of single, double, triple, and quadruple bonds.[30]

SPECTROSCOPY

I.II.1 Absorption spectroscopy:

The majority of physical techniques used to investigate inorganic compounds involve the absorption and sometimes the re-emission of electromagnetic radiation. The frequency of the radiation absorbed provides useful information on the energy levels of an inorganic compound and the intensity of the absorption can often be used to provide quantitative analytical information. Absorption spectroscopy techniques are normally nondestructive as after the measurement the sample can be recovered for further analysis.

I.II.2 Ultraviolet–visible spectroscopy:

Ultraviolet–visible spectroscopy (UV–visible spectroscopy) is the observation of the absorption of electromagnetic radiation in the UV and visible regions of the spectrum. It is sometimes known as electronic spectroscopy because the energy is used to excite electrons to higher energy levels. UV–visible spectroscopy is among the most widely used techniques for studying inorganic compounds and their reactions, and most laboratories possess a UV–visible spectrophotometer Fig.4

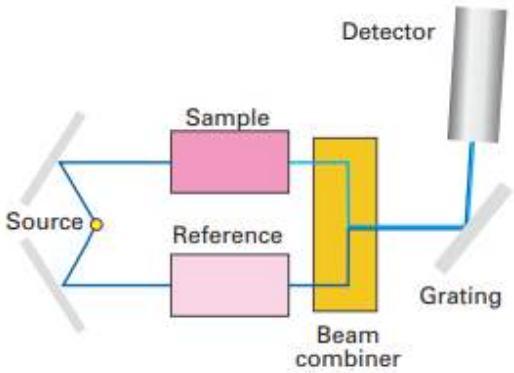

Fig.4 The layout of a typical UV-visible absorption spectrometer

I.II.2.1 Measuring a spectrum:

The sample for a UV–visible spectrum determination is usually a solution but may also be a gas or a solid. A gas or liquid is contained in a cell (a ‘cuvette’) constructed of an optically transparent material such as glass or, for UV spectra at wavelengths below 320 nm, pure silica. Usually, the beam of incident radiation is split into two, one passing through the sample and the other passing through a cell that is identical except for the absence of the sample. The emerging beams are compared at the detector (a photodiode) and the absorption is obtained as

a function of wavelength. Conventional spectrometers sweep the wavelength of the incident beam by changing the angle of a diffraction grating, but it is now more common for the entire spectrum to be recorded at once using a diode array detector. For solid samples, the intensity of UV–visible radiation reflected from the sample is more easily measured than that transmitted through a solid and an absorption spectrum is obtained by subtraction of the reflected intensity from the intensity of the incident radiation.

The intensity of absorption is measured as the absorbance, A, defined as

$$A = \log_{10}\left(\frac{I_0}{I}\right)$$

where I_0 is the incident intensity and I is the measured intensity after passing through the sample. The detector is the limiting factor for strongly absorbing species because the measurement of low photon flux is unreliable.

The empirical Beer–Lambert law is used to relate the absorbance to the molar concentration [J] of the absorbing species J and optical pathlength L:

$$A = \varepsilon\,[J]L$$

where ε (epsilon) is the molar absorption coefficient (still commonly referred to as the 'extinction coefficient' and sometimes the 'molar absorptivity'). Values of ε range from above 10^5 $dm^3\,mol^{-1}\,cm^{-1}$ for fully allowed transitions, for example an electron transferring from the 3d to 4p energy levels in an atom ($\Delta l = 1$), to less than 1 $dm^3\,mol^{-1}\,cm^{-1}$ for 'forbidden' transitions, such as those with ($\Delta l = 0$). Selection rules also exist for transitions between molecular orbitals, although in complex molecules they are frequently broken. For small molar absorption coefficients, the absorbing species may be difficult to observe unless the concentration or pathlength is increased accordingly.

Figure 8.11 shows a typical solution UV–visible spectrum obtained from a d-metal compound, in this case Ti(III), which has a d^1 configuration. From the wavelength of the radiation absorbed, the energy levels of the compound, including the effect of the ligand environment on d-metal atoms, can be inferred. The type of transition involved can often be inferred from the value of ε. The proportionality between absorbance and concentration provides a way to

measure properties that depend on concentration, such as equilibrium compositions and the rates of reaction.

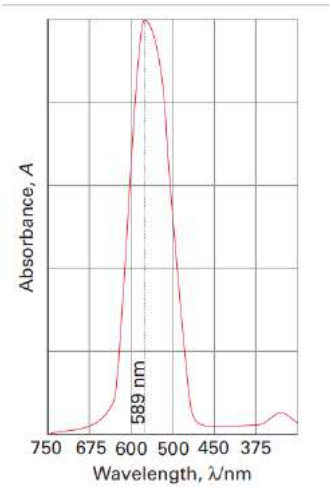

Fig.5 The UV–visible absorption spectrum of the solid ultramarine blue $Na_7[SiAlO_4]_6(S_3)$

I.II.2.2 The Absorption Process

The absorption law, also known as the Beer-Lambert law or just Beer's law, tells us quantitatively how the amount of attenuation depends on the concentration of the absorbing molecules and the path length over which absorption occurs. As light traverses a medium containing an absorbing analyte, the intensity decreases as the analyte becomes excited. For an analyte solution of a given concentration, the longer the length of the medium through which the light passes (path length of light), the more absorbers are in the path, and the greater the attenuation. Similarly, for a given path length of light, the higher the concentration of absorbers, the stronger the attenuation.

I.II.3 Selection rules and intensities:

The contrast in intensity between typical charge-transfer bands and typical ligand-field bands raises the question of the factors that control the intensities of absorption bands. In an octahedral, nearly octahedral, or square-planar complex, the maximum molar absorption coefficient ε_{max} (which measures the strength of the absorption) is typically less than or close to $100\ dm^3\ mol^{-1}\ cm^{-1}$ for ligand-field transitions. In tetrahedral complexes, which have no centre of symmetry, ε_{max} for ligand-field transitions might exceed $250\ dm^3\ mol^{-1}\ cm^{-1}$. By contrast, charge-transfer bands usually have an ε_{max} in the range $1000-50\ 000\ dm^3\ mol^{-1}\ cm^{-1}$

To understand the intensities of transitions in complexes we have to explore the strength with

which the complex couples with the electromagnetic field. Intense transitions indicate strong coupling; weak transitions indicate feeble coupling. The strength of coupling when an electron makes a transition from a state with wavefunction ψ_i to one with wavefunction ψ_i is measured by the transition dipole moment, which is defined as the integral

$$\mu_{fi} = \int \psi^*_f \, \mu \psi_i \, d\tau$$

where μ is the electric dipole moment operator, $-er$. The transition dipole moment can be regarded as a measure of the impulse that a transition imparts to the electromagnetic field: a large impulse corresponds to an intense transition; zero impulse corresponds to a forbidden transition. The intensity of a transition is proportional to the square of its transition dipole moment. A spectroscopic selection rule is a statement about which transitions are allowed and which are forbidden. An allowed transition is a transition with a nonzero transition dipole moment, and hence nonzero intensity. A forbidden transition is a transition for which the transition dipole moment is calculated as zero. Formally forbidden transitions may occur in a spectrum if the assumptions on which the transition dipole moment were calculated are invalid, such as the complex having a lower symmetry than assumed.

I.II.4 Spin selection rules:

The electromagnetic field of the incident radiation cannot change the relative orientations of the spins of the electrons in a complex. For example, an initially antiparallel pair of electrons cannot be converted to a parallel pair, so a singlet (S = 0) cannot undergo a transition to a triplet (S = 1). This restriction is summarized by the rule $\Delta S = 0$ for spin-allowed transitions, figure 5. The coupling of spin and orbital angular momenta can relax the spin selection rule, but such spin-forbidden, $\Delta S \neq 0$, transitions are generally much weaker than spin-allowed transitions. The intensity of spin-forbidden bands increases as the atomic number increases because the strength of the spin-orbit coupling is greater for heavy atoms than for light atoms. The breakdown of the spin selection rule by spin-orbit coupling is often called the heavy-atom effect. In the 3d series, in which spin-orbit coupling is weak, spin-forbidden bands have ε_{max} less than about 1 $dm^3\ mol^{-1}\ cm^{-1}$; however, spin-forbidden bands are a significant feature in the spectra of heavy d-metal complexes.[31]

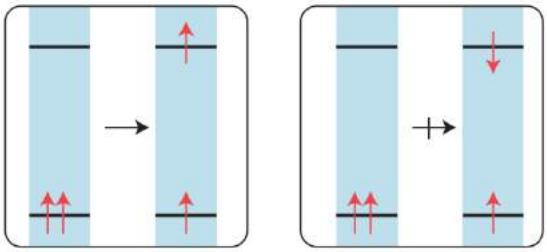

(a) **(b)**

Fig.6 (a) A spin-allowed transition does not change the multiplicity. **(b)** A spin-forbidden transition results in a change in the multiplicity.

I.II.5 Types of molecular transitions:

I.II.5.a σ→σ* Transitions:

This transition needs high energy, it is very strong and occurs in saturated hydrocarbons such as (methane, ethane …), and this transition requires very short radiation of wavelength (high energy)

I.II.5.b n→σ* Transitions:

This type of transition occurs in saturated compounds which containing one heteroatom has unshared pair electron such as (alcohols, ethers). Energy of n→σ* transition less than energy of σ→σ* transition

$I.II.5.c\ \pi \rightarrow \pi^*$ Transitions:

This type of transition occurs in unsaturated compounds. This types occurs at longer of wavelength than σ→σ* transition. Alkenes, alkynes and carbonyl compounds contain this transition

$I.II.5.d\ n \rightarrow \pi^*$ transition:

This type of transition occurs in unsaturated compounds which containing heteroatom has unshared pair electron. Unshared electron (n) on heteroatom excited to (π *) level. Energy of $n \rightarrow \pi^*$ transition less than energy of other transition and occurrence at longer wavelengths.[32]

I.II.5.e *d*−*d* transitions:

For a *d*-metal complex the surrounding crystal field (or ligand field) can introduce a non-spherical potential, which can break the degeneracy in the *d* orbitals. In an octahedral complex, such as $\left[\mathrm{Ti}(OH_2)_6\right]^{3+}$ the five degenerate *d* orbitals are split as shown below.

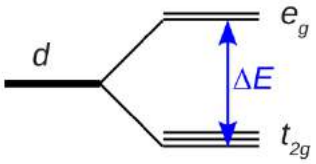

Fig.7 Electronic energy levels and transitions

The energy difference ΔE is the crystal field splitting. The order of the orbitals depends on the symmetry of the crystal field. For example, in a tetrahedral complex the order of the e_g and t_{2_g} states is reversed. The crystal field splittings are typically rather small and hence these absorptions appear mainly in the visible region of the spectrum. For $\left[\mathrm{Ti}(OH_2)_6\right]^{3+}$ the splitting is about 20,000 cm^{-1} (500 nm) corresponding to about 2.5 eV.[33]

I.II.6 Charge-transfer transitions:

In a CT transition, an electron migrates between orbitals that are predominantly ligand in character and orbitals that are predominantly metal in character. The transition is classified as a ligand-to-metal charge-transfer transition (LMCT transition) if the migration of the electron is from the ligand to the metal, and as a metal-to-ligand charge-transfer transition (MLCT transition) if the charge migration occurs in the opposite direction.

I.II.6.a LMCT Transitions:

Ligand-to-metal charge-transfer transitions are observed in the visible region of the spectrum when the metal is in a high oxidation state and ligands contain nonbonding electrons; the variation in the position of LMCT bands can be parameterized in terms of optical electronegativities.

I.II.6.b MLCT Transitions:

Charge-transfer transitions from metal to ligand are observed when the metal is in a low oxidation state and the ligands have low-lying acceptor orbitals.[34]

I.II.7 Infrared spectroscopy:

Infrared spectroscopy is the subset of spectroscopy that deals with the infrared region of the electromagnetic spectrum. It covers a range of techniques, the most common being a form of absorption spectroscopy. It is widely used for the identification of organic compounds because of the fact that their spectra are generally complex and provide numerous maxima and minima that can be used for comparison purposes. Infrared spectroscopy is generally concerned with absorption 5 of infrared radiation incident on the sample. The IR technique when coupled with intensity measurements may be used for qualitative and quantitative analysis. Currently, this technique has become more popular when compared to other physical techniques (X-ray diffraction, electron spin resonance, etc.,) in the elucidation of the structure of unknown compounds.[35]

I.II.7.1 The techniques:

The IR vibrational spectrum of a compound is obtained by exposing the sample to infrared radiation and recording the variation of the absorbance with frequency, wavenumber, or wavelength.

In early spectrometers, the transmission was measured as the frequency of the radiation was swept between two limits. Now the spectrum is extracted from an interferogram by Fourier transformation, which converts information in the time domain (based on the interference of waves travelling along paths of different lengths) to the frequency domain. The sample must be contained in a material that does not absorb IR radiation, which means that glass cannot be used and aqueous solutions are unsuitable unless the spectral bands of interest occur at frequencies not absorbed by water. Optical windows are typically constructed from CsI. Traditional procedures of sample preparation include KBr pellets (where the sample is diluted with dried KBr and then pressed into a translucent disc) and paraffin mulls (where the sample is produced as a suspension that is then placed as a droplet between the optical windows). These methods are still widely used, although becoming more popular are total internal reflectance devices in which the sample is simply placed in position. A typical range of an IR spectrum is between 4000 and 250 cm^{-1}, which corresponds to a wavelength of electromagnetic radiation of between

2.5 and 40 μm; this range covers many important vibrational modes or inorganic bonds. Fig.7 shows a typical spectrum.

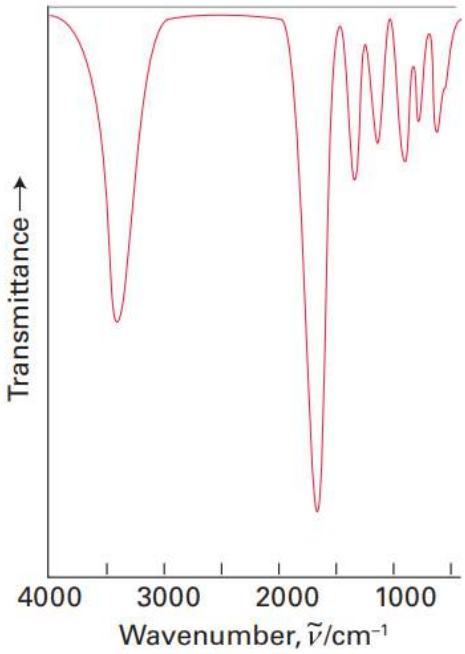

Fig.8 The IR spectrum of nickel acetate tetrahydrate showing characteristic absorptions due to water and the carbonyl group (OH stretch at 3600 cm^{-1} and C = 0 stretch at c.1700 cm^{-1}).

I.II.8 Nuclear magnetic resonance:

Nuclear magnetic resonance is suitable for studying compounds containing elements with magnetic nuclei, especially hydrogen. The technique gives information on molecular structure, including chemical environment, connectivity, and internuclear separations. It also probes molecular dynamics and is an important tool for investigating rearrangement reactions occurring on a millisecond timescale.

NMR is the most powerful and widely used spectroscopic method for the determination of molecular structures in solution and pure liquids. In many cases it provides information about shape and symmetry with greater certainty than is possible with other spectroscopic techniques, such as IR and Raman spectroscopy. It also provides information about the rate and nature of the interchange of ligands in fluxional molecules and can be used to follow reactions, in many cases providing exquisite mechanistic detail. The technique has been used to obtain the structures of protein molecules with molar masses of up to 30 kg mol^{-1} (corresponding to a molecular mass of 30 kDa) and complements the more static descriptions obtained with X-ray

single-crystal diffraction. However, unlike X-ray diffraction, NMR studies of molecules in solution generally cannot provide precise bond distances and angles, although it can provide some information on internuclear separations. It is a nondestructive technique because the sample can be recovered from solution after the resonance spectrum has been collected.[36]

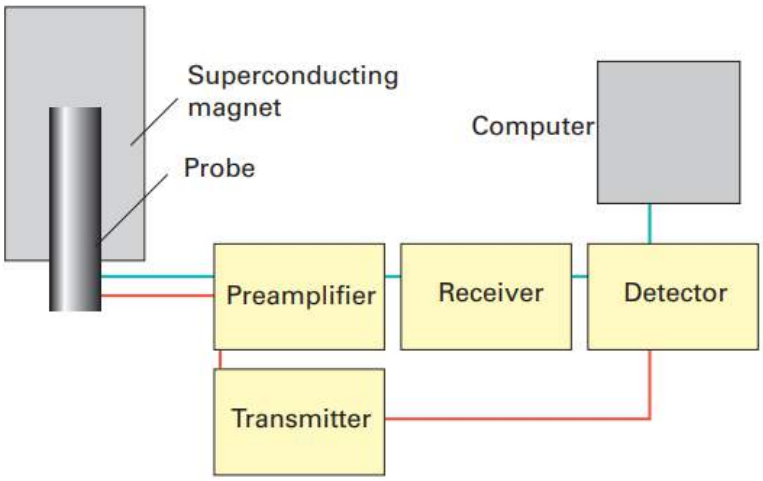

Fig.9 The layout of a typical NMR spectrometer

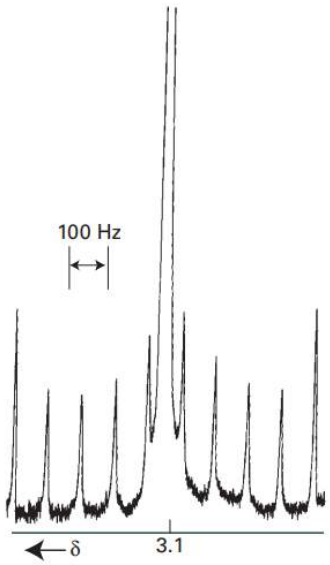

Fig.10 The ^{1}H-NMR spectrum of GeH_4

Chapter II

Methodology

Computational
Methods

II.1 The Schrödinger Equation:

In 1926, the Austrian physicist Erwin Schrödinger proposed an equation for finding the wavefunction of any system. The time-independent Schrödinger equation for a particle of mass *m* moving in one dimension with energy *E* is

$$-\frac{h^2}{2m}\frac{d^2\Psi}{dx^2}+V(x)\Psi=E\Psi$$

The factor V(x) is the potential energy of the particle at the point x; because the total energy E is the sum of potential and kinetic energies, the first term must be related (in a manner we explore later) to the kinetic energy of the particle; ħ(which is read h-cross or h-bar) is a convenient modification of Planck's constant:

$$\hbar = \frac{h}{2\pi} = \ 1.054\ 57 \times 10^{-34}\ \text{Js}$$

For a partial justification of the form of the Schrödinger equation, see the Justification below. The discussions later in the chapter will help to overcome the apparent arbitrariness of this complicated expression. For the present, treat the equation as a quantum-mechanical postulate. Various ways of expressing the Schrödinger equation, of incorporating the time-dependence of the wavefunction, and of extending it to more dimensions, are collected in Table

Table 01: The Schrödinger equation

For one-dimensional systems:

$$-\frac{\hbar^2}{2m}\frac{d^2\Psi}{dx^2} + V(x)\Psi = E\Psi$$

Where V(x) is the potential energy of the particle and E is its total energy. For three-dimensional systems

$$-\frac{\hbar^2}{2m}\nabla^2\Psi + V\Psi = E\Psi$$

where V may depend on position and ∇2 (‘del squared’) is

$$\nabla^2 = \frac{\partial^2}{\partial x^2}\frac{\partial^2}{\partial y^2}\frac{\partial^2}{\partial z^2}$$

In systems with spherical symmetry three equivalent forms are

$$\nabla^2 = \frac{1}{r}\frac{\partial^2}{\partial r^2}r + \frac{1}{r^2}r\wedge^2$$

$$= \frac{1}{r^2}\frac{\partial}{\partial r}r^2\frac{\partial}{\partial r} + \frac{1}{r^2}\wedge^2$$

$$= \frac{\partial^2}{\partial r^2}r + \frac{2}{r}\frac{\partial}{\partial r} + \frac{1}{r^2}\wedge^2$$

Where

$$\wedge^2 = \frac{1}{sin^2\theta}\frac{\partial^2}{\partial\varphi^2} + \frac{1}{\sin\theta}\frac{\partial}{\partial\theta}\sin\theta\frac{\partial}{\partial\theta}$$

In the general case the Schrödinger equation is written

$$\hat{H}\Psi = E\Psi$$

where $\hat{H}$ is the hamiltonian operator for the system:

$$\hat{H} = -\frac{\hbar^2}{2m}\nabla^2 + V$$

For the evolution of a system with time, it is necessary to solve the time-dependent Schrödinger equation

$$\hat{H}\Psi = ih\frac{\partial \Psi}{\partial t}$$

In quantum mechanics, a wavefunction that describes the spatial distribution of a particle (a 'spatial wavefunction') is complex if the particle it describes has a net motion. In the present case, we can use the relation

$$e^{i\theta} = \cos\theta + i\sin\theta$$

To write

$$\psi = \cos kx + i\sin kx$$

The real and imaginary parts of ψ are drawn in Fig, and we see that the imaginary component $\mathrm{Im}(\psi) = \sin kx$ is shifted in the direction of the particle's motion. That is, both the real and imaginary parts of the wavefunction are 'real', in the sense of being present, and we express ψ as a complex function simply to help with the visualization of the motion of the particle the wavefunction desribes. Now we recognize that *cos kx* (or *sin kx*) is a wave of wavelength

$\lambda = 2\pi/k$, as can be seen by comparing cos kxwith the standard form of a harmonic wave, $\cos(2\pi x/\lambda)$. The quantity E − V is equal to the kinetic energy of the particle, E_K, so

$k = (2mE_K/\hbar^2)^{1/2}$, which implies that $E_K = k^2\hbar^2/2m$. Because $E_K = p^2/2m$, it follows that

$$p = k/\hbar$$

Therefore, the linear momentum is related to the wavelength of the wavefunction by

$$P = \frac{2\pi}{\lambda} \times \frac{h}{2\pi} = \frac{h}{\lambda}$$

Which is the de Broglie relation.[37]

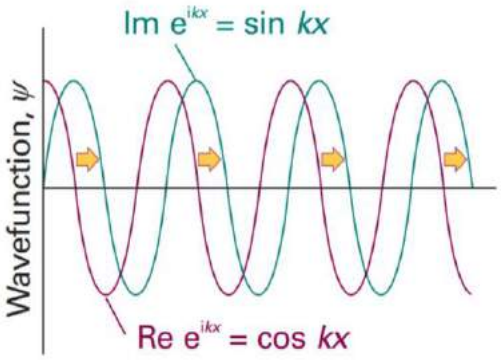

Fig.1 The real (purple) and imaginary (blue) parts of a free particle wavefunction corresponding to motion towards positive x (as shown by the arrow)

II.2 Density Functional Methods: (DFT)

The basis for Density Functional Theory (DFT) is the proof by Hohenberg and Kohn1 that the ground state electronic energy is determined completely by the electron density ρ. In other words, there exists a one-to-one correspondence between the electron density of a system and the energy.

The significance of the Hohenberg–Kohn theorem is perhaps best illustrated by comparing it with the wave function approach. A wave function for an N electron system contains 4N variables, three spatial and one spin coordinate for each electron.The electron density is the square of the wave function, integrated over N − 1 electron coordinates, and each spin density only depends on three spatial coordinates, independent of the number of electrons. While the complexity of a wave function increases exponentially with the number of electrons, the electron density has the same number of variables, independent of the system size. The “only” problem is that although it has been proven that each different density yields a different ground state energy, the functional connecting these two quantities is not known. The goal of DFT methods is to design functionals connecting the electron density with the energy.

A note on semantics: a function is a prescription for producing a number from a set of variables (coordinates). A functional is a prescription for producing a number from a function, which in turn depends on variables. A wave function and the electron density are thus functions, while the energy depending on a wave function or an electron density is a functional. We will denote a function depending on a set of variables with parenthesis, *f(x)*, while a functional depending on a function is denoted with brackets, *F*[*f*].

Early attempts at designing DFT models (actually predating wave mechanics) tried to express all the energy components as a functional of the electron density but these methods had poor performance, and wave function-based methods were consequently preferred. The success of modern DFT methods is based on the suggestion by Kohn and Sham in 1965 that the electron kinetic energy should be calculated from an auxiliary set of orbitals used for representing the electron density.5 The exchange–correlation energy, which is a rather small fraction of the total energy, is then the only unknown functional, and even relatively crude approximations for this term provide quite accurate computational models. The simplest model is the local density approximation, where the electron density is assumed to be slowly varying, such that the exchange–correlation energy can be calculated using formulas derived for a uniform electron density.A significant improvement in the accuracy can be obtained by making the exchange–correlation functional dependent also on the first derivative of the density, and further refinements also add the second derivative and mix Hartree–Fock exchange into the functional. Density functional theory is conceptually and computationally very similar to Hartree–Fock theory, but provides much better results and has consequently become a very popular method. The main problem in DFT is the inability to systematically improve the results, and the known failure to describe certain important features, such as van der Waals interactions.

II.2.1 Kohn–Sham Theory:

The foundation for the use of DFT methods in computational chemistry is the introduction of orbitals, as suggested by Kohn and Sham (KS). The main flaw in orbital-free models is the poor representation of the kinetic energy, and the idea in the KS formalism is to split the kinetic energy functional into two parts, one which can be calculated exactly, and a small correction term. The price to be paid is that orbitals are re-introduced, thereby increasing the complexity from 3 to 3N variables, and that electron correlation re-emerges as a separate term. The KS model is closely related to the HF method, sharing identical formulas for the kinetic, electron–nuclear and Coulomb electron–electron energies.

The division of the electron kinetic energy into two parts, with the major contribution being equivalent to the HF kinetic energy, can be justified as follows. Assume for the moment a Hamiltonian operator of the form in eq with $0 \leq l \leq 1$.

$$\mathbf{H}_\lambda = \mathbf{T} + \mathbf{V}_{ext}(\lambda) + \lambda \mathbf{V}_{ee}$$

The external potential operator V_{ext} is equal to V_{ee} for $\lambda = 1$, but for intermediate λ values it is assumed that $V_{ext}(\lambda)$ is adjusted such that the same density is obtained for $\lambda = 1$ (the real system), for $\lambda = 0$ (a hypothetical system with non-interacting electrons) and for all intermediates l values. For the $\lambda = 0$ case, the electrons are noninteracting, and the exact solution to the Schrödinger equation is given as a Slater determinant composed of (molecular) orbitals, φ, and the *exact* kinetic energy functional is given in eq

$$T_s = \sum_{i=1}^{N_{elect}} \langle \varphi_i | -\frac{1}{2}\nabla^2 | \varphi_i \rangle$$

The subscript S denotes that it is the kinetic energy calculated from a Slater determinant. The $\lambda = 1$ case corresponds to interacting electrons, and eq. is therefore only an approximation to the real kinetic energy.

Another way of justifying the use of eq. () for calculating the kinetic energy is by reference to natural orbitals. The exact kinetic energy can be calculated from the natural orbitals (NO) arising from the exact density matrix

$$T\left[\rho_{\text{exact}}\right] = \sum_{i=1}^{\infty} n_i \langle \varphi_i^{\text{NO}} | -\frac{1}{2}\nabla^2 | \varphi_i^{\text{NO}} \rangle$$

$$\rho_{\text{exact}} = \sum_{i=1}^{\infty} n_i \left| \varphi_j^{\text{NO}} \right|^2$$

$$N_{elec} = \sum_{i=1}^{\infty} n_i$$

The orbital occupation numbers ni (eigenvalues of the density matrix) will be between 0 and 1, corresponding to the number of electrons in the (spin) orbital. Representing the exact density will require an infinite number of natural orbitals, with the N_{elec} first having occupation numbers close to 1, and the remaining close to 0. Since the exact density matrix is not known, an (approximate) density can be written in terms of a set of auxiliary one-electron functions, i.e. orbitals.

$$\rho_{\text{approx}} = \sum_{i=1}^{N_{elec}} |\varphi_i|^2$$

The key to Kohn–Sham theory is to calculate the kinetic energy under the assumption of non-interacting electrons (in the same sense that HF orbitals in wave mechanics describe non-interacting electrons) from eq. (). In reality, the electrons are interacting, and eq. () does not provide the total kinetic energy. However, just as HF theory provides ~99% of the correct answer, the difference between the exact kinetic energy and that calculated by assuming non-interacting orbitals is small. The remaining kinetic energy is absorbed into an exchange–correlation term, and a general DFT energy expression can be written as in eq.!

$$E_{DFT}[\rho] = T_S[\rho] + E_{ne}[\rho] + J[\rho] + E_{xc}[\rho]$$

By equating EDFT to the exact energy, this expression defines Exc, i.e. it is the part that remains after subtraction of the non-interacting kinetic energy, and the Ene and J potential energy terms.

$$E_{xc}[\rho] = \left(T[\rho] - T_S[\rho]\right) + \left(E_{ee}[\rho] - J[\rho]\right)$$

The first parenthesis in eq. () may be considered as the kinetic correlation energy, while the last contains both potential correlation and exchange energy. The task in developing orbital-free models is to derive approximations to the kinetic, exchange and correlation energy functionals, while the corresponding task in Kohn–Sham theory is to derive approximations to the exchange–correlation energy functional only. For the neon atom, for example, the kinetic energy is 128.9 au, the exchange energy is −12.1 au, and the correlation energy is −0.4 au (as calculated by wave mechanics methods). Since the exchange–correlation energy is roughly a factor of 10 smaller than the kinetic energy, Kohn–Sham theory is much less sensitive to inaccuracies in the functional(s) than orbital-free theory. While orbital-free theory is a true density functional theory (three variables), Kohn–Sham methods are independentparticle

models (3N variables), analogous to Hartree–Fock theory, but are still much less complicated than many-particle (correlation) wave function models.[38]

II.3 Functionals:

When Kohn and Sham proposed their approach in 1965, they had already mentioned the interest in that an exact treatment of the exchange could have. They had already established an expression of the exchange-correlation energy based on the Hartree-Fock approximation for the exchange, the correlation term remaining unchanged compared to the LDA. They had also noted that the actual potential would have, through the use of this functional hybrid, a correct asymptotic behavior (in 1/r) away from the atom. This idea was born shown to be effective in treating atoms but has led to disappointing results on molecules. In the vast majority of cases, the GGAs were able to achieve greater accuracy.

The reason for this failure is the artificial nature of the separation of the terms of trade and correlation: by combining a non-local exchange hole (Hartree-Fock) with a local correlation (LDA), the autocoherence of the description of the local hole has been lost.

Becke has therefore chosen to use the exact exchange differently by including only a part of it in the exchange-correlation energy[21]. To this end, he proposed an expression to this effect three parameters which will be designated by B3[22]:

$$E_{xc} = E_{xc}^{LDA} + a_0\left(E_x^{exact} - E_x^{LDA}\right) + a_x \Delta E_x^{B88} + a_c \Delta E_c^{PW91}$$

Where the coefficients a_0, a_x and a_c are determined in a semi-empirical manner by adjustment on the experimental data. Exact E_{xc} here represents the exact exchange energy obtained from of a Hartree-Fock calculation. In the first correction term, the value of the coefficient a_0 can be related to the "independent particles" character of the system. The following two terms allow gradient corrections to be optimized, both for exchange and for correlation. As such, the above equation represents the simplest way to take into account counts the exact exchange and finds the uniform electron gas limit. Thanks to this approximation, the accuracy on energies is even better than when generalized gradient corrections are used. It is now a variant of this approach, using Lee's approximation, Yang and Parr (LYP) rather than Perdew and Wang's, known as B3LYP, which is the most popular.

$$E_{xc}^{B3LYP} = a_0 E_x^{LDA} + (1-a_0) E_x^{exact} + a_1 \Delta E_x^{B88} + E_c^{LDA} + a_2\left(E_c^{LYP} + E_c^{LDA}\right)$$

Where $a_0 = 0.80,\ a_1 = 0.72\ et\ a_2 = 0.81$. Parameters a_0, a_1 and a_2 are semiempirical quantities determined by smoothing the formation heat of a standard assembly of molecules. This functional gives remarkably accurate results for a large number of systems.

It has also been shown that, unlike GGA, to correctly describe the magnetic properties of molecular compounds of transition metals and ligands. However, it is far from putting an end to the problems related to exchange and correlation in DFT.

A number of avenues are currently being explored to maximize the benefits of benefits of the exact exchange. On the one hand, Becke has built new functionalities taking into account both exchange and correlation. According to him, functionals based on the GGAs and incorporating a specific proportion of exact exchange have reached a limit.

Other functional features have also been developed by Perdew, Burke and Ernzerhof (PBE) on purely theoretical grounds. Their performance is quite comparable to that of semi-empirical functionalities currently in use and seem very promising for the study of magnetic properties. Current developments aim to correct a good time and again the problem of self-interaction and consider more general terms of order high in the development of the electron density gradient, thus constituting a new step following the GGAs. Hamprecht, Cohen, Tozer and Handy (HTCH) have developed a functional one that does not use a fraction of the exact exchange but which gives better results than B3LYP for many systems, concerning energies but also geometries. It is based on the reparameterization of a functional proposed by Becke and has recently undergone improvements to expand its scope of application.

Note: In this work we used PBE0 and B3pw9.

II.4 Hartree-Fock self-consistent field method:

Even approximate methods for many-electron atoms become very complicated to treat with a pen and paper. Fortunately, modern computers can be programmed to solve this type of problems efficiently. Such approach relies heavily on the methods of numerical analysis. In 1928 Douglas Hartree introduced the self-consistent field (SCF) method. This method can be used to calculate an approximate wavefunction and energy for any ground-state atom (or molecule). If the inter-electron repulsion terms in the Schrödinger equation are ignored, the n-electron equation can be separated into *n* one-electron equations (just like was done for He). The approximate wavefunction is then a product of the one-electron wavefunctions (orbitals).

Douglas Hartree (1897 - 1958) English physicist Hartree used a symmetric variational wavefunction corresponding to a product of the orbital functions φi:

$$\psi = \varphi_1\varphi_2 \ldots \varphi_n$$

where each orbital satisfies the hydrogenlike Schrödinger equation (i.e. just one electron):

$$-\frac{h^2}{2m_e}\Delta\varphi_i(x, y, z) + V_i(x, y, z)\varphi_i(x, y, z) = \varepsilon_i\varphi_i$$

where ε_i is the energy of the orbital i. There are n such equations for each electron in the atom (or molecule). The effective potential V_i depends on other orbitals and hence the n equations are coupled and must be solved iteratively. For the exact form of the potential, see Molecular Quantum Mechanics (3rd ed.) by Atkins and Friedman. The SCF process is continued until the orbitals and their energies no longer change during the iteration. Note that the Hartree approach is missing two important effects: antisymmetry of the wavefuinction and so called electron correlation (not discussed further here). The antisymmetry is required by the Pauli principle.

In 1930 Fock and Slater concluded that the wavefunction must be antisymmetric and the Hartree method should employ the Slater determinant form, which includes spin orbitals. This method is referred to as the Hartree-Fock (HF) method. There are number of methods (computationally very demanding) that can include electron correlation on top of the HF model (configuration interaction (CI) and coupled clusters (CC); Computational methods typically employ a set of Gaussian functions for describing the orbitals ("basis set"). The larger the basis set, the better results it gives but at the expense of computer time. These basis sets are typically expressed with various acronyms like STO-3G, 3-21G, 6-311G*, etc.[39]

II.5 Time-Dependent Density-Functional Theory (TDDFT):

TDDFT is the most promising approach for describing the dynamics of interacting many-electron systems.[40]

We begin with the full time-dependent Schrödinger equation without any external vector potentials,

$$i\frac{\partial}{\partial t}\Psi(r_1, \ldots, r_N, t) = \left\{\sum_{j=1}^{N}\left[-\frac{\nabla_j^2}{2} + V(r_j, t)\right] + \frac{1}{2}\sum_{j\neq 1}^{N}\frac{1}{|r_j - r_i|}\right\}\Psi(r_1, \ldots, r_N, t)$$

Equation (5) is, in general, impossible to solve, even with the most advanced computational resources. At present, this can be done only for small systems, consisting of not more than two interacting electrons in three dimensions[41], or a few more interacting electrons in lower dimensions[42]. Any realistic time-dependent calculation of larger systems requires approximations. The key point is to cast the time-dependent many-body problem into a different form which is still formally exact but which makes it easier to develop approximations that are both accurate and computationally efficient.

TDDFT is based on the Runge-Gross theorem[43], which establishes a one-toone correspondence, $V(r,t) \leftrightarrow n(r,t)$, between time-dependent potentials and time-dependent single-particle densities: for a given initial many-body state Ψ_0, two different potentials $V(r,t)$ and $V'(r,t)$ (where "different" means that they are not just shifted by a purely time-dependent function) will always cause the system to evolve in time such that the respective time-dependent densities, $n(r,t)$ and $n'(r,t)$, are different. This one-to-one correspondence implies that the time-dependent density,

$$n(r,t) = N \int d^3 r_2 \ldots \int d^3 r_N \left|\Psi(r, r_2, \ldots, r_N, t)\right|^2$$

formally carries the same information as the potential. But the potential determines the time evolution of the system! Thus, the Hamiltonian, and hence the wave function, formally become a functional of the density, $\Psi[n](r_1,\ldots, r_N,t)$. As a consequence, all physical observables are, at least formally, expressible as density functionals:

$$O[n](t) = \left\langle \Psi[n](t) \middle| \hat{O}(t) \middle| \Psi[n](t) \right\rangle .$$

The remaining problem is to obtain the time-dependent density without actually having to solve the full time-dependent Schrödinger equation (otherwise, nothing would have been gained!). The idea is the following: instead of solving the time-dependent Schrödinger equation of the interacting system, we solve the time-dependent Schrödinger equation of a noninteracting system that produces the same density as the interacting system. Such a system is much easier to deal with, since its many-body wave function is simply a Slater determinant,

$$\Phi(r_1,\ldots, r_N,t) = \frac{1}{\sqrt{N}} det\left\{\varphi_j\left(r_j,t\right)\right\} ,$$

and we only need to solve a single-particle Schrödinger equation to obtain the time-dependent orbitals $\varphi_j(r,t)$:

$$i\frac{\partial}{\partial t}\varphi_j(r,t)=\left[-\frac{\nabla^2}{2}+Vs[n](r,t)\right]\varphi_j(r,t)$$

Here is a very important point to keep in mind: the time-dependent Kohn-Sham orbitals are designed to reproduce the exact density of the interacting system, i.e.

$$n(r,t)=\sum_{j=1}^{N}\left|\varphi_j(r,t)\right|^2$$

In other words, the Kohn-Sham system is not meant to reproduce the full many-body wave function of the interacting system, only its single-particle density. The time-dependent Kohn-Sham equation features an effective single-particle potential whose task is to cause the noninteracting system to reproduce the exact density. It is usually written in the following form:

$$V_s(r,t)=V(r,t)\ +\int d^3r'\ \frac{n(r',t)}{|r-r'|}+V_{xc}(r,t)$$

that is, as sum of the given potential V of the physical, interacting system, plus the time-dependent Hartree potential VH plus the time-dependent exchange-correlation (xc) potential Vxc. The latter two potentials are functionals of the density, so the time-dependent Kohn-Sham equation has to be solved self-consistently.

Readers who are familiar with ground-state density-functional theory (DFT)[44] will immediately be familiar with TDDFT as well, because both theories—DFT and TDDFT—are based on very similar premises. Indeed, the parallels are obvious:

The Runge-Gross theorem is the time-dependent counterpart of the Hohenberg-Kohn theorem[45], and the time-dependent Kohn-Sham equation is a generalization of the static Kohn-Sham approach[46]. However, there are important differences as well, and there are features of TDDFT that are unique to the time-dependent case:

• Ground-state DFT is based on the variational minimum principle. In the timedependent case, there is no analogous minimum principle. It is possible to derive the formal framework of TDDFT from a stationary-action principle[47 48]. But in contrast with DFT, where the ground-state energy E0 is the quantity of central importance, the action is practically of no interest in itself. • Mathematically, the Kohn-Sham equation of ground-state DFT

$$\left[-\frac{\nabla^2}{2}+V_S^0[n_0](r)\right]\varphi_j^0(r)=\varepsilon_j\varphi_j^0(r)$$

is a boundary-value problem, where the static effective potential V_S^0 depends selfconsistently on the ground-state density n_0(r). By contrast, the time-dependent Kohn-Sham equation (9) represents an initial-value problem. One proceeds in three steps:

1. Prepare the initial state, which is usually the ground state (technically, one can start from any initial state, but non-ground-state or non-stationary initial states are rarely considered). This means that one needs to carry out a static Kohn-Sham calculation for the system of interest, i.e., solve Eq. (9), to get a set of ground-state Kohn-Sham orbitals $\varphi_j^0(r)$ and orbital energies ε_j.

2. Solve the time-dependent Kohn-Sham equation (9) from the initial time t_0 to the desired final time t_1, where $\varphi_i(r,t_0)=\varphi_j^0(r)$ are the initial orbitals. The time propagation of the orbitals gives the time-dependent density n(r,t).

3. Calculate the desired observable(s) as functionals of n(r,t).

• The static xc potential is defined as

$$V_{xc}^0[n_0](r)=\left.\frac{\delta E_{xc}[n]}{\delta n(r)}\right|_{n_0(r)}$$

The common strategy for deriving approximations of V_{xc}^0 is to start with an approximation for the xc energy E_{xc} and then obtain the xc potential via Eq. (14). By contrast, the time-dependent xc potential is approximated directly.

• The time-dependent xc potential $V_{xc}[n](r,t)$ has many features and exact properties that are analogous to those of the static xc potential: for instance, it must be self-interaction free, it must have the correct asymptotic −1/r behavior, and it must exhibit an overall discontinuity upon change of particle number[49]. However, there are also features that have no counterpart in static DFT and are truly dynamic. The most important one is that the time-dependent xc potential has a memory: $V_{xc}[n](r,t)$ at time t depends on densities n (r′, t′) at earlier times, where t′≤ t. This memory is, in principle, infinitely long-ranged.

• The most common approximation for the time-dependent xc potential is the adiabatic approximation, which ignores all memory effects:

$$V_{xc}^{adia}(r,t) = V_{xc}^{0,approx}[n0](r)\Big|_{n_0(r)\to n(r,t)}$$

Here, an approximate xc potential from static DFT, $V_{xc}^{0,approx}[n0](r)$, is evaluated with the instantaneous time-dependent density. This is, obviously, very convenient, because this means that we can simply and straightforwardly use our favorite approximation from static DFT in TDDFT. A widely used example is the adiabatic local-density approximation (ALDA).

II.5.1 Concluding remarks:

Today, the main area in which TDDFT is used is in theoretical chemistry, for calculating excitation energies and optical properties of large molecular systems. It has become a standard feature of many popular computer codes in quantum chemistry and materials science, and as such has reached a similar status for electron dynamics as DFT has for ground-state properties. In this article, we have presented the TDDFT formalism and its features and capabilities in a nutshell, with a special emphasis on successes and challenges in the nonlinear regime and for matter under extreme conditions. Even though it represents an approach that is in principle exact, in practice there are some things that TDDFT (with the currently available, state-of-the-art approximations and implementations) can do well, and other situations in which it faces difficulties. In particular, observables that are implicit functionals of the density remain a challenge, and continue to be the subject of active research and development. The description of dissipation in TDDFT is a subject of active research as well, although much progress has been made in our understanding and in constructing the appropriate formal framework. In spite of these challenges, there can be no doubt that TDDFT is the only method that is capable of dealing with the nonlinear, real-time dynamics of many interacting electrons driven by arbitrary external fields, or coupled to the ions via adiabatic or nonadiabatic molecular dynamics. Large-scale TDDFT numerical simulations of materials are now within reach, such as the recent study by Yabana and coworkers who simulated high-intensity fs laser pulses acting on crystalline solids and leading to dielectric breakdown. As our computational capabilities continue to increase, we can expect many more such applications of TDDFT in the area of materials science under a broad variety of extreme (or not so extreme) conditions.[50]

II.6 Oscillator strength:

In spectroscopy, oscillator strength is a dimensionless quantity that expresses the probability of absorption or emission of electromagnetic radiation in transitions between energy levels of an atom or molecule.[51] [52] The oscillator strength can be thought of as the ratio between the quantum mechanical transition rate and the classical absorption/emission rate of a single electron oscillator with the same frequency as the transition.[53]

The oscillator strength *f* of a transition is defined as:

$$f = \frac{|\vec{\mu}|^2}{|\vec{\mu}_{osc}|^2}$$

where $\vec{\mu}$ is the eletric tramsition dipole moment for the electronic transition and $\vec{\mu}_{osc}$ is the same quantity for an electron confined in a three-dimensional harmonic potential Strongly allowed transitions have values close to one and forbidden transitions close to zero. For example, typical singlet-triplet transitions have $f \approx 10^{-5}$.

We established the connection between transition dipole moment $|\vec{\mu}|^2$ and the integrated molar absorption coefficient. Solving for $|\vec{\mu}|^2$ gives:

$$|\vec{\mu}|^2 = \frac{2.303 \times 3hc\varepsilon_0}{2\pi^2 N_A \nu_{12}} \int_{band} \varepsilon(\nu) d\nu$$

For an harmonic oscillator the transition dipole between two levels is:

$$|\vec{\mu}_{osc}|^2 = \frac{3he^2}{8\pi^2 m_e \nu_{12}}$$

When Eqs. (6.502) and (6.503) are inserted into Eq. (6.501) we get:

$$f = \frac{|\vec{\mu}|^2}{|\vec{\mu}_{osc}|^2} = \frac{2.303 \times 4m_e c\varepsilon_0}{N_A e^2} \int_{band} \varepsilon(\nu) d\nu$$

If the electron can be promoted to many different excited levels, the total oscillator strength is normalized to unity:[54]

$$\sum_{states} f_i = 1$$

II.7 The Gaussian Distribution:

The Gaussian distribution for the probability of random events is

$$p(x) = \frac{1}{\sqrt{2\pi}\sigma} \exp\left(-\frac{(x_i - \mu)^2}{2\sigma^2} \right)$$

It is widely used in experimental chemistry, most commonly in statistical treatment of experimental uncertainty (Young, 1962). For convenience, it is common to make the substitution

$$z = \frac{x_i - \mu}{\sigma}$$

With this substitution, distributions having different m and s can be compared by using the same curve, frequently called the normal curve

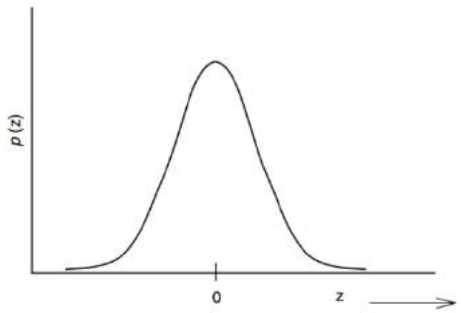

Fig.2 The Gaussian Normal Distribution

The integral of the Gaussian distribution function does not exist in closed form over an arbitrary interval, but it is a simple matter to calculate the value of p(z) for any value of z, hence numerical integration is appropriate. Like the test function $f(x) = 100 - x^2$, the accepted value

(Young, 1962) of the definite integral is approached rapidly by Simpson's rule. We have obtained four-place accuracy or better at millisecond run time. For many applications in applied probability and statistics, four significant figures are more than can be supported by the data. The iterative loop for approximating an area can be nested in an outer loop that prints the area under the Gaussian distribution curve for each of many increments in z. If the output is arranged in appropriate rows and columns, a table of areas under one half of the Gaussian curve can be generated, for example, from 0.0 to 3.0 z, resulting in printed values of the area at intervals of 0.01 z.

This is suggested to the interested reader as an exercise. We generated a 400-entry table in a negligible run time. The Gaussian function is symmetrical, so knowing one half of the curve means that we know the other half as well.[55]

II.8 Basis Set:

A basis set is a set of mathematical functions (basis functions), linear combinations of which yield molecular orbitals. The functions are usually, but not invariably, centered on atomic nuclei. Approximating molecular orbitals as linear combinations of basis functions is usually called the LCAO or linear combination of atomic orbitals approach, although the functions are not necessarily conventional atomic orbitals: they can be any set of mathematical functions that are convenient to manipulate and which in linear combination give useful representations of MO's. With this reservation, LCAO is a useful acronym. Physically, several (usually) basis functions describe the electron distribution around an atom and combining atomic basis functions yields the electron distribution in the molecule as a whole. Basis functions not centered on atoms (occasionally used) can be considered to lie on "ghost atoms"

II.8.1 Pople basis sets:

The notation for the split-valence basis sets arising from the group of John Pople is typically X-YZg.[56] In this case, X represents the number of primitive Gaussians comprising each core atomic orbital basis function. The Y and Z indicate that the valence orbitals are composed of two basis functions each, the first one composed of a linear combination of Yprimitive Gaussian functions, the other composed of a linear combination of Z primitive Gaussian functions. In this case, the presence of two numbers after the hyphens implies that this basis set is a split-valence double-zeta basis set. Split-valence triple- and quadruple-zeta basis sets are also used, denoted as X-YZWg, X-YZWVg, etc.

The 6-31G* basis set (defined for the atoms H through Zn) is a valence double-zeta polarized basis set that adds to the 6-31G set six *d*-type Cartesian-Gaussian polarization functions on each of the atoms Li through Ca and ten *f*-type Cartesian Gaussian polarization functions on each of the atoms Sc through Zn.

Pople basis sets are somewhat outdated, as correlation-consistent or polarization-consistent basis sets typically yield better results with similar resources. Also note that some Pople basis sets have grave deficiencies that may lead to incorrect results.[57]

II.8.2 Correlation-consistent basis sets:

Ones of the most widely used basis sets are those developed by Dunning and coworkers, since they are designed for converging Post-Hartree–Fock calculations systematically to the complete basis set limit using empirical extrapolation techniques.

For first- and second-row atoms, the basis sets are cc-pVNZ where N=D,T,Q,5,6,... (D=double, T=triples, etc.). The 'cc-p', stands for 'correlation-consistent polarized' and the 'V' indicates they are valence-only basis sets. They include successively larger shells of polarization (correlating) functions (*d*, *f*, *g*, etc.). More recently these 'correlation-consistent polarized' basis sets have become widely used and are the current state of the art for correlated or post-Hartree–Fock calculations. Examples of these are:

- cc-pVDZ - Double-zeta
- cc-pVTZ - Triple-zeta
- cc-pVQZ - Quadruple-zeta
- cc-pV5Z - Quintuple-zeta, etc.
- aug-cc-pVDZ, etc. - Augmented versions of the preceding basis sets with added diffuse functions.
- cc-pCVDZ - Double-zeta with core correlation

II.8.3 6–31G*:

The 6–31G* is probably the most popular basis at present. It gives good geometries and, often, reasonable relative energies; however, there seems to be little evidence that it is, in general, much better than the 3–21G* basis for geometry optimizations. Since it is about five times as slow as the 3–21G* basis, the general preference for the 6–31G* for geometry optimizations

may be due to its better relative energies. The 3–21G* basis does have certain geometry deficiencies compared to the 6–31G*, particularly its tendency to overzealously flatten nitrogen atoms (the N of aniline is wrongly predicted to be planar), and this, along with inferior relative energies and less consistency, may be responsible for its being neglected in favor of the 6–31G* basis set. Note that the geometries and energies referred to here are those from Hartree–Fock-level calculations. Post-Hartree–Fock calculations, which can give significantly better geometries and much better relative energies, are considered to require a basis set of at least the 6–31G* size for meaningful results. The 6–31G* basis adds polarization functions only to so-called heavy atoms (those beyond helium). Sometimes it is helpful to have polarization functions on the hydrogens as well; a 6–31G* basis with three 2p functions on each H and He atom (in addition to their 1s0 and 1s00 functions) is called the 6–31G** (or 6–31(d,p)) basis. The 6–31G* and 6–31G** bases are the same except that in the 6–31G** each H and He has five, rather than two, functions.

The 6–31G** basis probably offers little advantage over the 6–31G* unless the hydrogens are engaged in some special activity like hydrogen bonding or bridging [58].

EXPERIMENTAL
METHODS AND TECHNIQUES

In this chapter, you will find details about the experimental techniques, analytical procedures and materials, also the preparation of ligand and syntheses complex.

II.I.1 Materials and solvents employed:

2-benzoylpyridine	Sigma Aldrich
Ethylenediamine	
glacial acetic acid	Biochem Chemopharma
CuCl2.2H2O	Sigma Aldrich
CoCl2.6H2O	Sigma Aldrich
Ethanol absolute	Sigma Aldrich
Methanol absolute	Biochem Chemopharma
Diethyl ether	PubChem Chemopharma

II.I.2 Experimental methods:

II.I.2.a Preparation of Ligand:

The preparation of ligand LB were synthesized by a modification of the described method of Gourbatsis, S., et al.[59] a warm ethanolic solution of 2-benzoylpyridine (3.7 g, 20 mmol) with ethanolic solution of ethylenediamine (0.6 g, 10 mmol) in the presence of a few drops of glacial acetic acid. The reaction mixture turned red and refluxed for 6 h according to Fig.3. After this time, the resultant solution was poured into ice cold water and pale brown precipitate of the Schiff base separated out and filtered, washed with water and recrystallized from ethanol. The product characterised by ^{1}H NMR (see below).

Pale brown solid, yield (3.63 g, 46 %). m.p: 121-123 °C, chemical formula $C_{26}H_{22}N_4$ Mw 390.51 ^{1}H NMR (300 MHz, $CDCl_3$) δ 8.91 – 8.58 (m, J = 4.1, 8H), 7.69 – 7.18 (m, 10H), 3.81 (t, 4H). ^{13}C NMR (75MHz, $CDCl_3$) δ 55.26, 54.77, 124.6, 137.09, 148.47, 150.03, 169.06

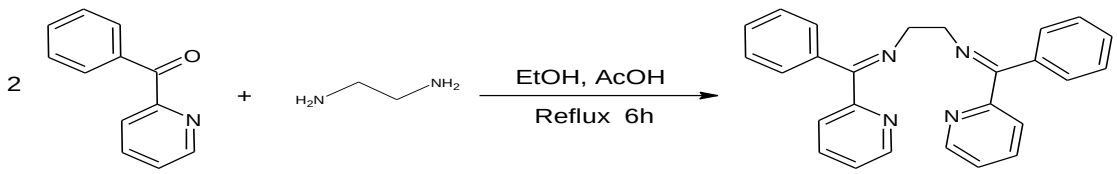

Fig.3 Synthesis of ligand LB. (reaction conditions and reagents)

Fig.4 Schiff base *ligand LB*

II.I.2.b Preparation of the complexes:

All the metal complexes in this work were prepared using a 1:1 metal salt:ligand molar ratio.

II.I.2.b.1 Synthesis of Copper (II) Complexe:

A solution of $CuCl_2.2H_2O$ (0.21 g, 1.2 mmol) in methanol (5 cm^3) was added dropwise to an equimolar solution of LB (0.5 g, 1.2 mmol) in methanol (10 cm^3). The mixture was stirred at room temperature for 3 hours. The colorless solution turned green and formed a precipitate, The green precipitate was filtered, washed with methanol and Et_2O to remove unreacted ligand. Yield: (0.51 g, 89 %).

Fig.5 Solid of Cu (II) Complexe

II.I.2.b.2 Synthesis of Cobalt (II) Complexe:

The cobalt complexe [CoLCl2] was obtained by adding dropwise a solution of $CoCl_2.6H_2O$ (0.16 g, 1.2 mmol) in THF (5 cm^3) to a solution of LB (0.35 g, 1.3 mmol) in THF (10 cm^3). The mixture was heated at 60 °C for 5 hours. The colorless solution turned red and then a brown precipitate formed and was filtered off, washed with THF and Et_2O to remove the unreacted ligand. Yield: (0.44 g, 78 %).

Fig.4 powder of Co (II) Complexe

In the next chapter, we studied a complex theoretically, that complex have been synthesized by Lai Qin Chai and coworkers. [10] And about our complexes and ligand we just characterized them with IR and NMR.

Chapter III

Results and Discussion

Theoretical

Results

III.1 Study of geometrical structures:

III.1.1 In DMF Solvent:

The geometrical parameters of our complex [Ni$(L)_2$] have been optimized at the DFT level with two functionals B3pw91 and PBE0.The (Ni) metal electrons have been described with the LanL2DZ basis set, while other atoms' (H, C, O, N, Cl) have been described with 6-31+G** basis set. All Calculations have been done in the presence of DMF solvent (ε= 36,71).The solvent effects were taken into account by the PCM model. The obtained results are presented in the table.1. The optimized structure (Fig.1) is an octahedral with some distortion, the same as the experimental structure. The two functionals are in a good agreement with the experience except two bonds, Ni-$N_1$and Ni-O_2. The reason is that there are two dihedral angles (C_{23}-C_{22}-N_7-C_{31}) and (C_{22}-C_{21}-C_{20}-N_6) which have some distortion. With regard to the other angles the error between the calculated and the experimental values is acceptable. (Table.1)

III.1.2 In DCM Solvent:

The geometrical parameters of our complex [Ni ($L)_2$] have been optimized at the DFT level with two functionalB3pw91 and PBE0.The (Ni) metal electrons have been described with the Lan L2DZ basis set, while other atoms' (H, C, O, N, Cl) with 6-31+G**.All Calculations have been done in the presence of DCM solvent (ε= 8.93).The solvent effects were taken into account by the PCM model. The obtained results are presented in the table below Table.1. The optimized structure (Fig.1) is an octahedral with some distortion, the same as the experimental studied structure. The two functionals are in a good agreement with the experience except two bonds, Ni-$N_1$and Ni-O_2. The reason is that there are two dihedral angles (C_{23}-C_{22}-N_7-C_{31}) and (C_{22}-C_{21}-C_{20}-N_6) which have some distortion, with regard to the other angles the error between the calculated and the experimental value is acceptable. Table.1.

Table.1 Selected bond distances (Å) and angles (°) for the [Ni (L)2] complex

DMF				DCM			
Bounds	Pbe0	B3pw91	Exp	Bounds	Pbe0	B3pw91	Exp
(Ni-N_1)	2.640	2.800	2.130	(Ni-N_1)	2.645	2.791	2.130
(Ni-N_2)	1.927	1.926	2.010	(Ni-N_2)	1.928	1.928	2.010
(Ni-N_3)	1.913	1.918	2.046	(Ni-N_3)	1.913	1.918	2.046
(Ni-N_4)	1.897	1.901	2.041	(Ni-N_4)	1.897	1.900	2.041
(Ni-O_1)	1.892	1.893	1.999	(Ni-O_1)	1.890	1.891	1.999
(Ni-O_2)	2.357	2.385	2.043	(Ni-O_2)	2.344	2.375	2.043
Angle	Pbe0	B3pw91	Exp	Angle	Pbe0	B3pw91	Exp
N_1-Ni-N_2	69.0	70.5	79.8	N_1-Ni-N_2	42.7	69.9	79.8
N_1-Ni-N_3	100.1	97.4	94.4	N_1-Ni-N_3	100.2	97.8	94.4
N_1-Ni-N_4	99.6	93.3	92.0	N_1-Ni-N_4	100.1	94.1	92.0
N_2-Ni-N_3	169.1	167.6	172.8	N_2-Ni-N_3	168.9	167.4	172.8
N_2-Ni-N_4	95.1	96.5	101.2	N_2-Ni-N_4	95.0	96.4	101.2
N_3-Ni-N_4	87.4	86.8	83.0	N_3-Ni-N_4	87.5	86.8	83.0
N_1-Ni-O_1	89.7	95.7	97.4	N_1-Ni-O_1	89.0	94.7	97.4
N_1-Ni-O_2	157.3	159.4	169.5	N_1-Ni-O_2	156.3	158.4	169.5
N_2-Ni-O_1	93.1	92.9	89.7	N_2-Ni-O_1	93.1	92.9	89.7
N_2-Ni-O_2	89.0	88.9	91.0	N_2-Ni-O_2	88.4	88.5	91.0
N_3-Ni-O_1	85.5	85.2	86.7	N_3-Ni-O_1	85.5	85.2	86.7
N_3-Ni-O_2	101.5	103.0	94.9	N_3-Ni-O_2	102.3	103.6	94.9
N_4-Ni-O_1	169.1	168.6	166.5	N_4-Ni-O_1	169.3	168.7	166.5
N_4-Ni-O_2	87.5	87.3	84.5	N_4-Ni-O_2	87.8	87.5	84.5
C_{22}-C_{21}-C_{20}-N_6	5.1	-34.5	20.8	C_{22}-C_{21}-C_{20}-N_6	5.93	-31.6	20.8
C_{23}-C_{22}-N_7-C_{31}	59.5	70.9	45.2	C_{23}-C_{22}-N_7-C_{31}	59.8	70.9	45.2

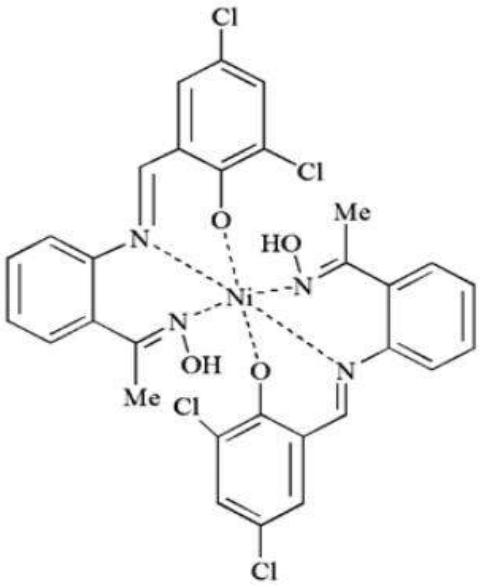

Fig.1 [Ni($L^{2)}_2$] complex [10]

III.2 Frontier molecular orbitals:

Frontier molecular orbitals FMOs energies and their composition in terms of fragment orbitals of the studied complexes are given in the tables.2 and 3 respectively. HOMO, H-1, LUMO and L+1 isosurfaces of the studied complex are given in scheme 1. HOMO and H-1 orbitals of the studied complex are mainly delocalized on the phenolate rings and on d-metal orbitals. It should be noted that the d-metal orbitals percentage obtained with B3pw91is more important than the one obtained with Pbe0 in both solvents DMF and DCM. The unoccupied orbitals LUMO and L+1 are overall delocalized on $\pi^*_{Phenolate}$. While L+3 and L+4 orbitals are delocalized on π^* of quinazoline. The L+2 orbital is contributed by d-metal and slightly by $\pi^*_{quinazoline}$. Computed energy gaps of the studied complex in the two solvents are almost equal, while calculated energy gaps with both functionals B3pw91 and Pbe0 are overall different.

Table.2 Energies and character of FMOs of the complex NiL_2.

DCM					
PBE0			B3PW91		
OM	ε (ev)	Character (%)	OM	ε (ev)	Character (%)
L + 4	-1.240	76% $\pi_{quinazoline}$	L + 4	-1.388	85% $\pi_{quinazoline}$
L + 3	-1.434	73%$\pi_{quinazoline}$+ 22%$\pi_{Phenolate}$	L + 3	-1.624	73% $\pi_{quinazoline}$ + 24% $\pi_{Phenolate}$
L + 2	-1.724	50% dNi	L + 2	-2.007	55% dNi
L + 1	-2.084	72% $\pi_{Phenolate}$	L + 1	-2.282	25% $\pi_{Phenolate}$ + 50% $\pi_{Phenolate}$ + 20% $\pi_{quinazoline}$
LUMO	-2.210	53% $\pi^*_{Phenolate}$ +28%$\pi_{quinazoline}$	**LUMO**	-2.350	17% $\pi^*_{Phenolate}$ + 61% $\pi^*_{Phenolate}$
ΔE	3.451		**ΔE**	3.129	
HOMO	-5.661	82% $\pi^*_{Phenolate}$+ 11%dNi	**HOMO**	-5.479	72% $\pi^*_{Phenolate}$ + 21% dNi
H - 1	-6.010	40%dNi+ 38% $\pi_{Phenolate}$	H - 1	-5.658	39% dNi + 46%$\pi_{Phenolate}$
H - 2	-6.353	71%$\pi_{Phenolate}$+ 12%dNi	H - 2	-6.182	74% $\pi_{Phenolate}$ + 17% dNi
H - 3	-6.835	39%$\pi_{quinazoline}$+ 37% $\pi_{quinazoline}$	H - 3	-6.604	50% $\pi_{quinazoline}$+ 22% dNi
H- 4	-6.985	51% $\pi_{quinazoline}$ + 27%$\pi_{quinazoline}$	H - 4	-6.797	85% $\pi_{quinazoline}$
H - 5	-7.212	48% $\pi_{Phenolate}$ + 28% $\pi_{quinazoline}$	H - 5	-6.999	49% $\pi_{Phenolate}$ + 28% $\pi_{quinazoline}$ + 16% dNi
H - 6	-7.346	43% $\pi_{Phenolate}$ + 28% $\pi_{quinazoline}$ + 19%$\pi_{quinazoline}$	H - 7	-7.140	36% $\pi_{Phenolate}$ + 30% $\pi_{Phenolate}$ + 25 dNi
H - 7	-7.471	51% $\pi_{Phenolate}$ + 24% $\pi_{quinazoline}$ + 17% dNi	H - 8	-7.268	50% $\pi_{quinazoline}$ + 18% $\pi_{Phenolate}$ + 15%dNi
H - 8	-7.547	34%dNi + 29% $\pi_{quinazoline}$ + 21%$\pi_{quinazoline}$			
H - 9	-7.764	48% dNi+ 25% $\pi_{quinazoline}$			

Table.3 Energies and character of FMOs of the complex NiL_2.

DMF					
PBE0			B3PW91		
OM	ε (ev)	Characters	OM	ε (ev)	Characters
L + 4	-1.234	77% $\pi_{quinazoline}$	L + 4	-1.355	87% $\pi_{quinazoline}$
L + 3	-1.439	74%$\pi_{quinazoline}$+ 21% $\pi_{Phenolate}$	L + 3	-1.633	73% $\pi_{quinazoline}$ + 23% $\pi_{Phenolate}$
L + 2	-1.744	51% dNi + 18% $\pi_{quinazoline}$	L + 2	-2.033	56% dNi
L + 1	-2.113	70% $\pi_{Phenolate}$	L + 1	-2.309	22% $\pi_{Phenolate}$ + 52% $\pi_{Phenolate}$ + 20% $\pi_{quinazoline}$
LUMO	-2.232	52% $\pi^*_{Phenolate}$ +27% $\pi^*_{quinazoline}$+ 17% $\pi_{Phenolate}$	**LUMO**	-2.384	16% $\pi^*_{Phenolate}$ + 64% $\pi^*_{quinazoline}$
ΔE	3.478		**ΔE**	3.147	
HOMO	-5.710	81%$\pi^*_{Phenolate}$+ 12%dNi	**HOMO**	-5.531	71% $\pi^*_{Phenolate}$ + 22% dNi
H - 1	-6.060	41%dNi+ 38% $\pi_{Phenolate}$	H– 1	-5.718	38% dNi + 47% $\pi_{Phenolate}$
H - 2	-6.399	70% $\pi_{Phenolate}$ + 11%dNi	H - 2	-6.239	73% $\pi_{Phenolate}$ + 18% dNi
H - 3	-6.840	35%$\pi_{quinazoline}$+44% $\pi_{quinazoline}$	H - 3	-6.625	50% $\pi_{quinazoline}$+ 20% dNi
H - 4	-6.997	44% $\pi_{quinazoline}$ +33%$\pi_{quinazoline}$	H - 4	-6.801	81% $\pi_{quinazoline}$
H - 5	-7.235	47%$\pi_{Phenolate}$+ 31%$\pi_{quinazoline}$	H - 5	-7.025	44%$\pi_{Phenolate}$+ 34%$\pi_{quinazoline}$ + 16% dNi
H - 6	-7.362	37% $\pi_{quinazoline}$ + 37% $\pi_{Phenolate}$ + 18%$\pi_{quinazoline}$	H - 7	-7.193	42% $\pi_{Phenolate}$+ 26%$\pi_{Phenolate}$ + 24% dNi
H - 7	-7.507	51% $\pi_{Phenolate}$+ 26%$\pi_{quinazoline}$ + 13%dNi	H - 8	-7.263	60% $\pi_{quinazoline}$+ 10% dNi
H - 9	-7.778	47%dNi+ 21%$\pi_{quinazoline}$			

Table.4 Energies, oscillator strengths, and character of the main absorption of the complex NiL_2, computed with B3PW91 and PBE0

DCM

B3PW91

State	λ(nm)	*f*	Transition	Character
S8	447	0.14	H-1→L+1 (52%) HOMO→L+1 (34%)	MLCT\LLCT
S11	386	0.0572	H-2→LUMO (77%)	LLCT\MLCT
S31	296	0.0925	H-7→L+1 (25%) H-5→L+1 (23%)	LLCT\MLCT
S36	283	0.1243	H-8→L+1 (14%) H-5→L+2 (15%)	LLCT\MLCT LMCT\MC

PBE0

State	λ(nm)	*f*	Transition	Character
S7	433	0.0913	H-1→LUMO (64%), HOMO→LUMO (26%)	MLCT\LLCT
S8	422	0.0664	H-1→L+1 (67%), HOMO→L+1 (26%)	MLCT\LLCT
S11	369	0.069	H-2→LUMO (43%), H-2→L+1 (21%)	LLCT\MLCT
S16	325	0.0599	H-3→LUMO (77%)	LLCT
S21	299	0.0564	H-7→LUMO (30%)	LLCT\MLCT
S23	296	0.0641	H-3→L+2 (60%)	LMCT\LLCT
S24	292	0.1329	H-5→LUMO (27%)	LLCT
S33	275	0.0814	H-6→L+1 (39%)	LLCT
S35	270	0.0746	H-9→LUMO (43%), H-6→L+1 (25%)	MLCT\LLCT
S36	268	0.0615	H-5→L+2 (21%), H-3→L+3 (27%)	LMCT\LLCT

DMF

B3PW91

State	λ(nm)	*f*	Transition	Character
S8	441	0.1346	H-1→L+1 (56%), HOMO→L+1 (32%)	MLCT\LLCT
S11	384	0.0529	H-2→LUMO (78%)	LLCT\MLCT
S15	344	0.0853	H-3→LUMO (59%), H-3→L+1 (21%)	MLCT\LLCT
S30	296	0.0736	H-5→L+1 (24%), H-7→L+1 (21%)	LLCT\MLCT
S35	283	0.0824	H-8→L+1 (18%), H-5→L+2 (13%), H-3→L+3 (11%)	LLCT\MLCT MC
S39	278	0.0934	H-3→L+3 (30%)	LLCT\MLCT

PBE0

State	λ(nm)	*f*	Transition	Character
S7	428	0.0769	H-1→LUMO (65%), HOMO→LUMO (24%)	MLCT\LLCT
S8	417	0.0736	H-1→L+1 (65%), HOMO→L+1 (26%)	MLCT\LLCT
S16	325	0.0589	H-3→LUMO (73%)	LLCT
S21	299	0.0588	H-7→LUMO (38%), H-5→LUMO (30%)	LLCT\MLCT LLCT
S24	291	0.148	H-5→LUMO (37%)	LLCT
S33	276	0.0629	H-9→LUMO (20%), H-6→L+1 (46%)	MLCT\LLCT
S34	271	0.0703	H-9→LUMO (44%), H-6→L+1 (25%)	MLCT\LLCT
S37	266	0.0881	H-9→L+1 (48%)	MLCT\LLCT

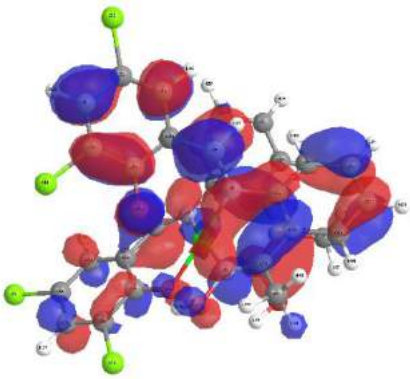

LUMO-DCM-pbe0

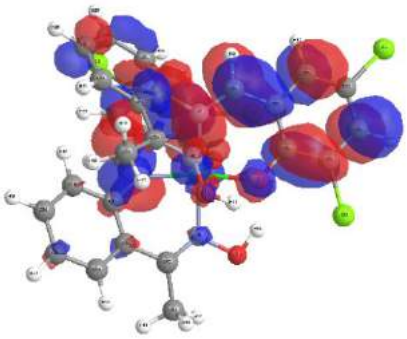

L+1-DCM-pbe0

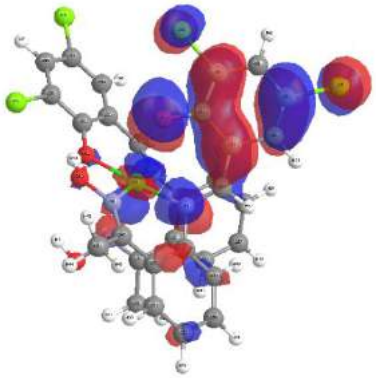

HOMO-DCM-pbe0

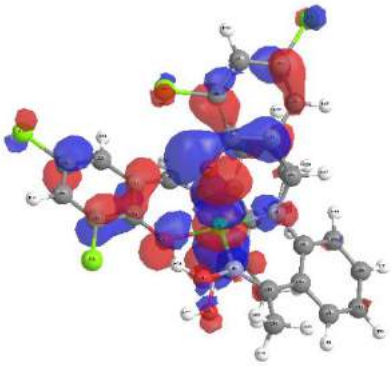

H-1-DCM-pbe0

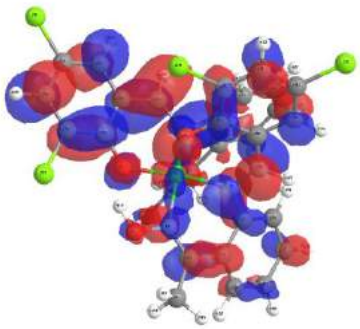

LUMO-DCM-b3pw91

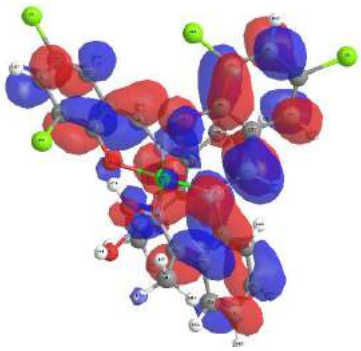

L+1-DCM-b3pw91

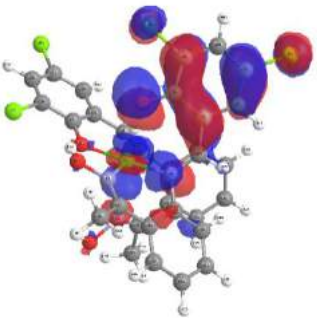

HOMO-DCM-b3pw91

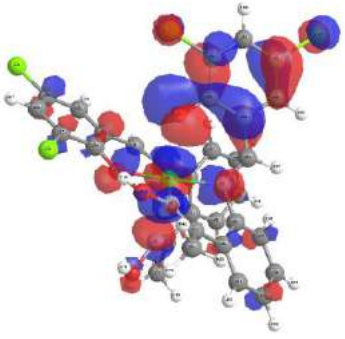

H-1-DCM-b3pw91

Fig.2 Isosurfaces in DCM solvent

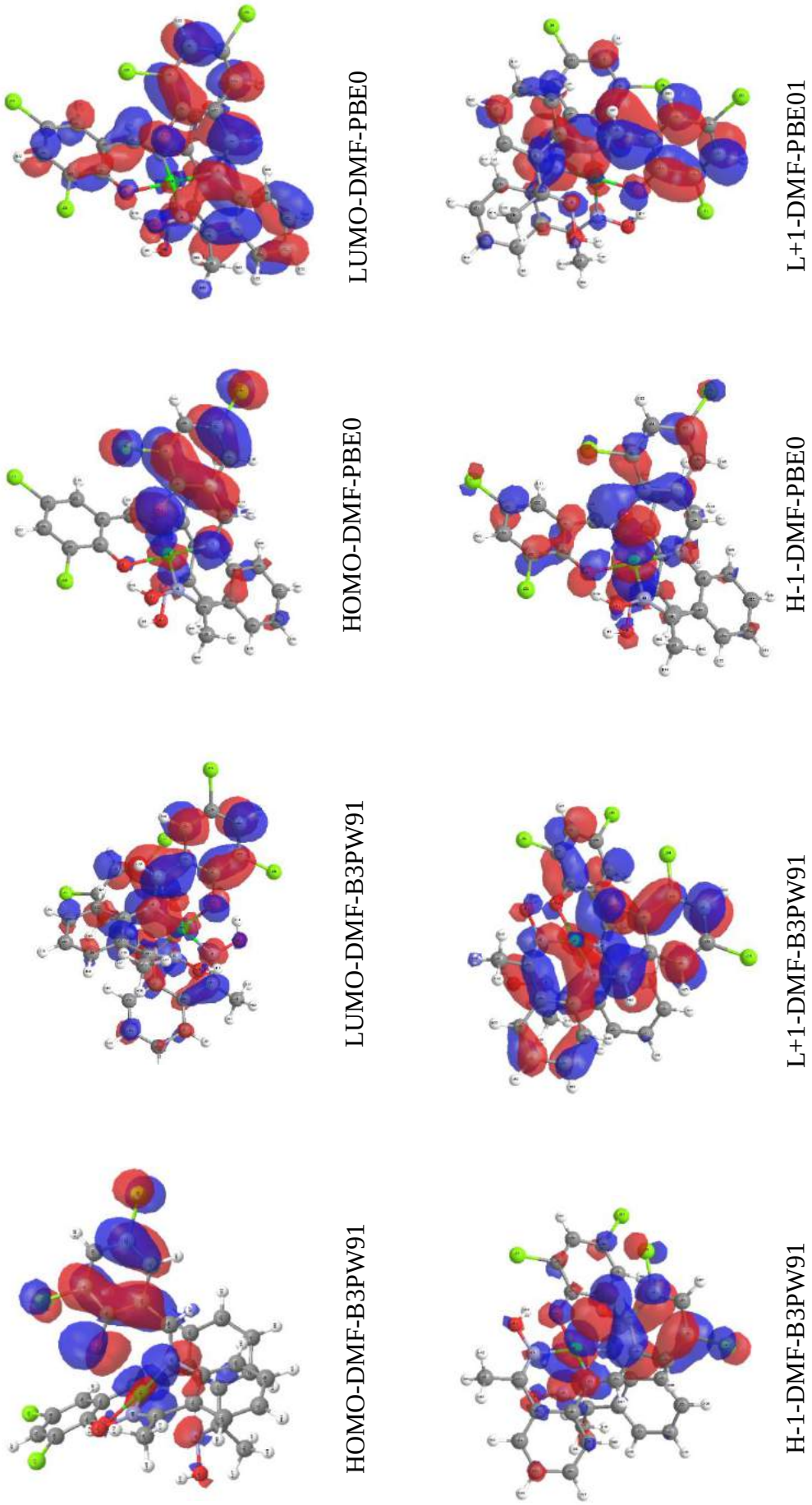

Fig.3 Isosurfaces in DMF solvent

III.3 Electronic absorption spectra:

III.3.1 With the dichloromethane (DCM):

The simulated absorption spectrum obtained with B3pw91 redshift the PBE0 one. Indeed, B3pw91 spectrum starts to absorb at ~556 nm, while PBE0 start around ~579 nm. However, PBE0 spectrum reproduced better the observed spectrum.In the visible region, the simulated PBE0 band is due to the transition S_0-S_7 calculated at (443 nm,f =0.0913), which has mixed (LLCT/MLCT) character. It's done from dNi $+\pi_{Phenolate}$ orbitales to $\pi^*_{Phenolate} + \pi^*_{quinazoline}$. A shoulder appear on the PBE0 spectrum at ~360 nm is contributed by the transition S_0-S_{11} (396 nm, f =0.069), wich has mixed (LLCT/MLCT) character. This shoulder is attributed to the observed shoulder around ~298 nm. In UV region, the intense band observed around ~249 nm can be assigned to the occurred band in the PBE0 spectrum ~284 nm, this band is contributed by the transitions group S_0-S_{23} (296 nm, f =0.0641); S_0-S_{24} (292 nm, f =0.1392) and S_0-S_{33}(275 nm, f =0.0814). This transitions have mainly an LLCT character. As the PBE0 spectrum is in a good agreement with the experience than the B3pw91 one, we will be discussing only the PBE0 spectrum.

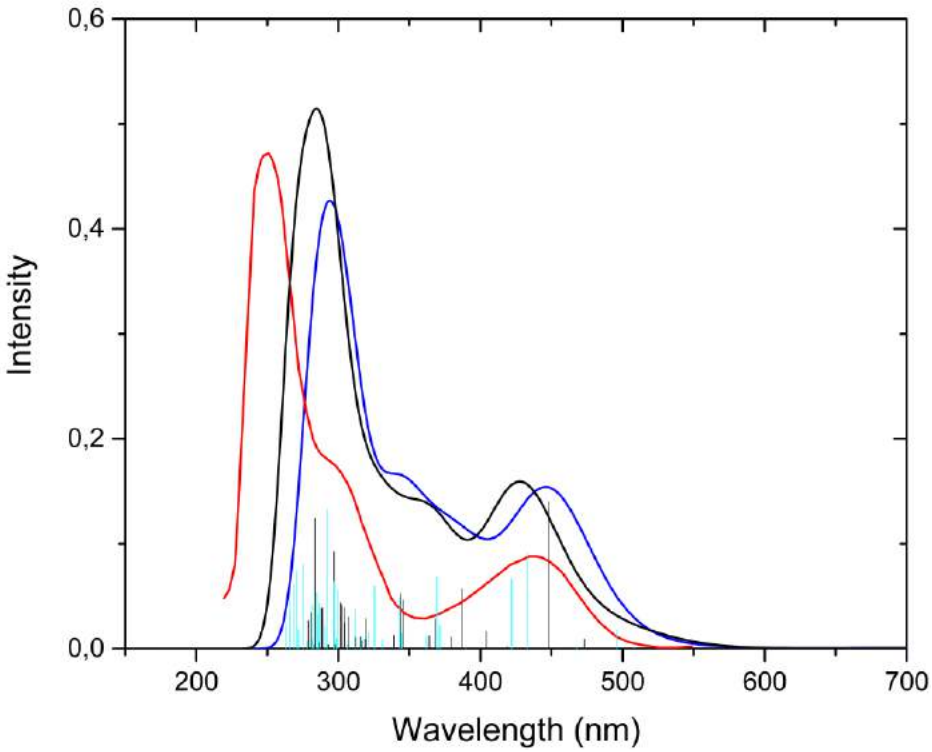

Fig.4 Simulated absorption spectra (solid lines) and calculated absorptions (bars) of the complex [NiL_2] obtained using B3PW91 (blue) and PBE0 (black) and the digitized experimental spectrum from [10] (red).

III.3.2 With the DMF:

The simulated absorption spectrum obtained with B3pw91 redshift the PBE0 one. Indeed, B3pw91 spectrum starts to absorb at ~565 nm, while PBE0 start around ~567 nm. However, PBE0 spectrum reproduced better the observed spectrum. In the visible region, the simulated PBE0 band is due to the transition S_0-S_7 calculated at (428 nm, f =0.0769), which has mixed (LLCT/MLCT) character. It's done from dNi $+\pi_{Phenolate}$ orbitales to $\pi^*_{Phenolate} + \pi^*_{quinazoline}$. A shoulder appear on the PBE0 spectrum at ~361 nm is contributed by the transition S_0-S_8 (417 nm, f =0.0736), wich has mixed (LLCT/MLCT) character. This shoulder is attributed to the observed shoulder around ~298 nm. In UV region, the intense band observed around ~249 nm can be assigned to the occurred band in the PBE0 spectrum ~284 nm, this band is contributed by the transitions group S_0-S_{24} (291nm, f =0.148); S_0-S_{33} (276 nm, f =0.0629) and S_0-S_{34} (271nm, f =0.0703). This transitions have mainly an LLCT character.

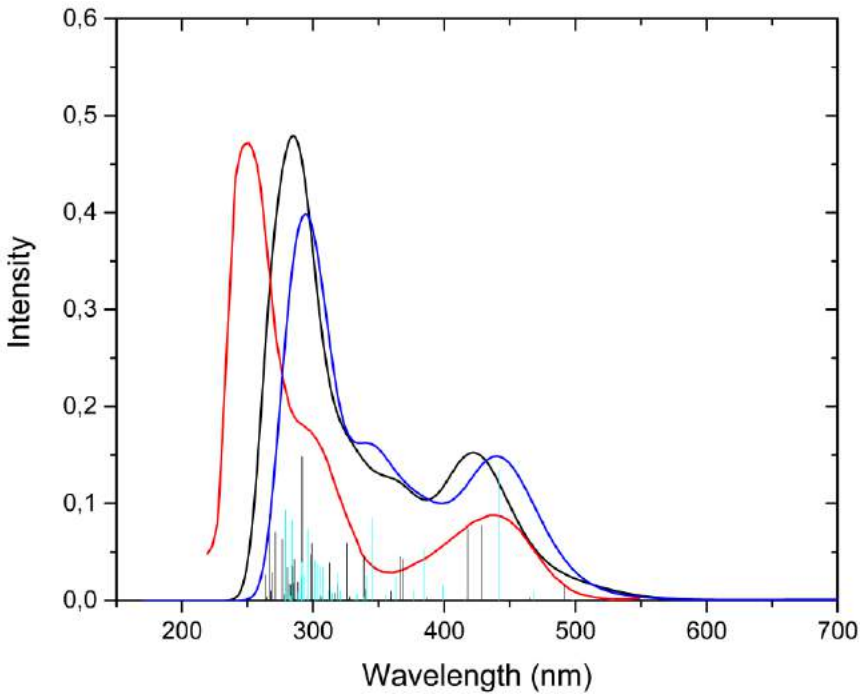

Fig.5 Simulated absorption spectra (solid lines) and calculated absorptions (bars) of the complex [NiL_2] obtained using B3PW91 (blue) and PBE0 (black) and the digitized experimental spectrum from [10] (red).

III.3.3 Comparative analysis:

In the Fig.6 we notice that the change of solvent did not greatly affect the simulated spectrum. In the visible region, the simulated spectrum with both functionals in DMF blueshift the simulated one in DCM. The simulated spectra are practically superimposed in the UV region.

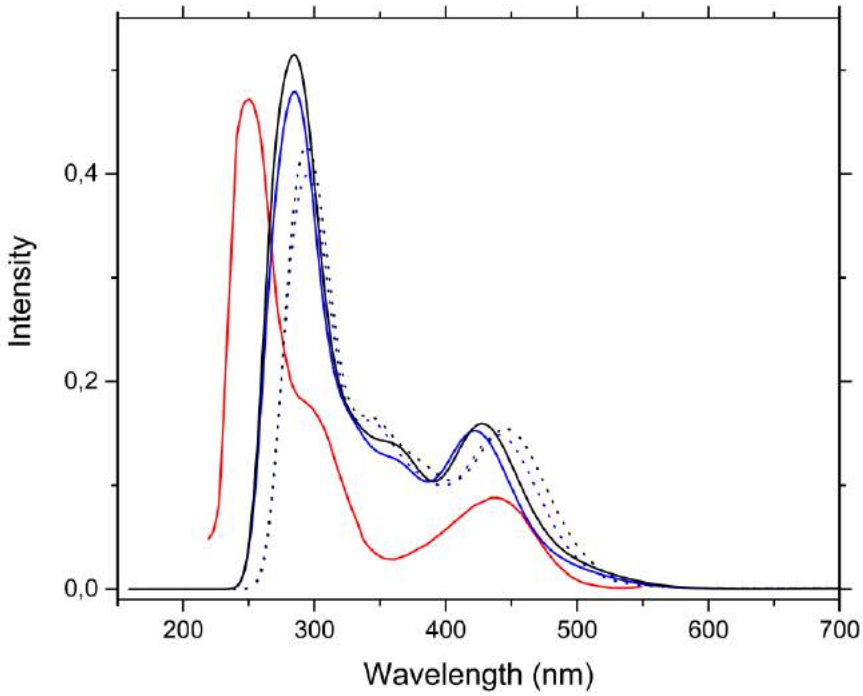

Fig.6 Simulated absorption spectra (solid and dotted lines) of the complex [NiL_2] obtained using B3PW91 (blue) and PBE0 (black) and the digitized experimental spectrum from [10] (red).

Experimental

Results

III.I.1 Characterization of ligand LB:

III.I.1.1 NMR spectra:

The ^{1}H NMR, spectrum of LB in $CDCl_3$ exhibits two triplets appear at δ 3.81 ppm corresponds to methylene groups, and nine groups of multiplet peaks between δ 7.06 and 8.91 ppm assigned to the ring's protons. The appearance of multiplet peaks for the methylene protons and the multiplicity of all signals assigned to the rings' protons.

III.I.2 Characterization of (Cu(II)) and (Co(II)) complexes:

III.I.2.1 Infrared spectra:

The infrared spectra were recorded on a PERKIN ELMER device series FTIR has transformed from Fourrier using a KBr pellet in which is dispersed our product (concentration 3% in 150 mg KBr) under a pressure of 80 tons/cm, were measured in a range of 400 – 4000cm-1.

Fig.7 spectrometer used IRTF 8300

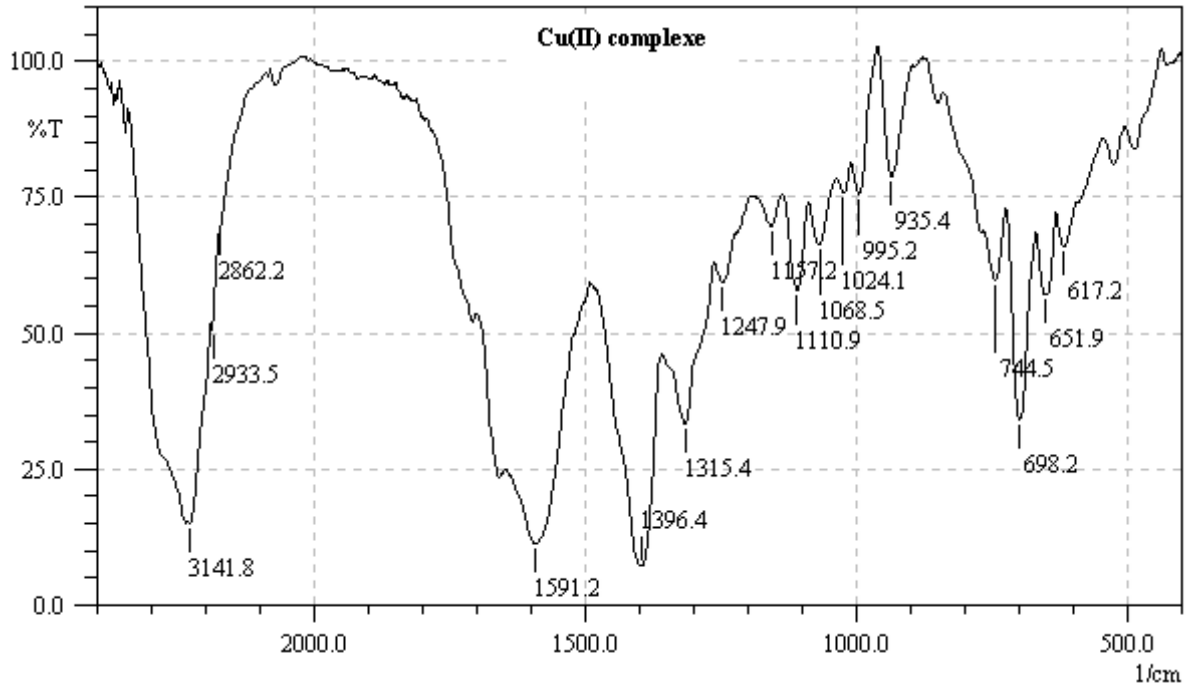

Fig.8 The IR spectra of Cu(II) complexe

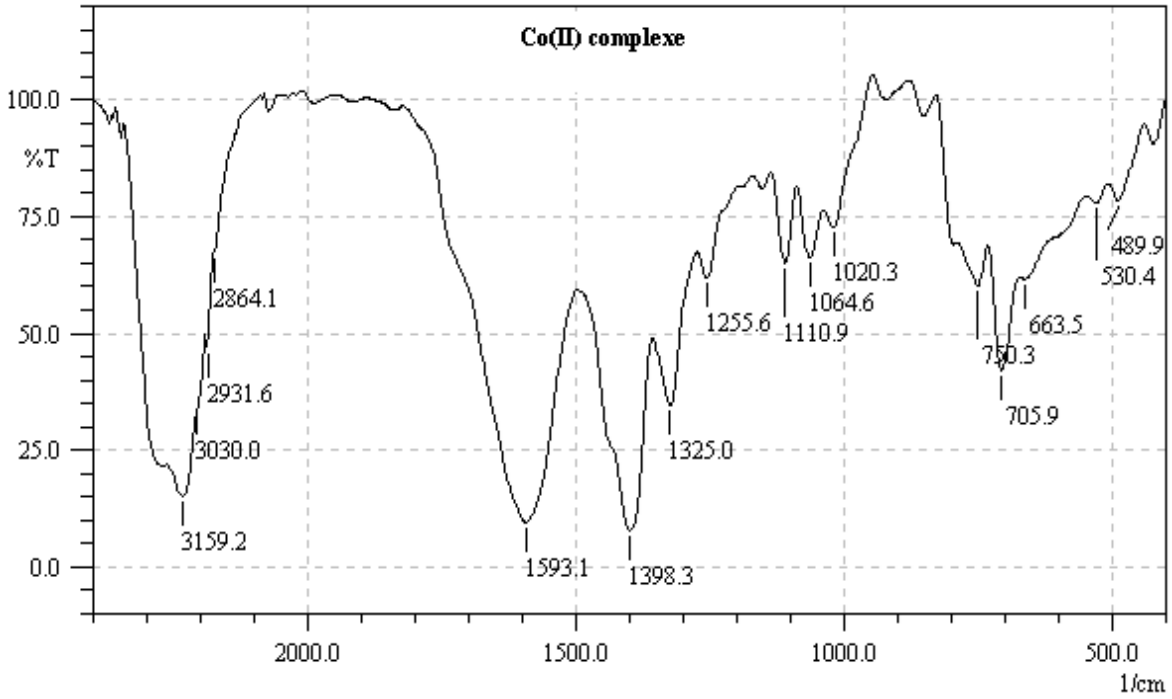

Fig.9 The IR spectra of Co(II) complexe

The main vibrational bands of complexes Cu(II), Co(II) are given in the experimental section and characteristic absorption bands listed are shown below in Table 5.

Table.5 Absorption Band with their Corresponding Vibrations (cm-1)

υ_{max} **(cm-1)**	**Cu(II) complexe**	**Co(II) complexe**
C-Hstr (SP^2 aromatic)	3141.8	3030-3159.2
C-Hstr (SP^3)	2862.2-2933.5	2864.1-2931.6
C=Nstr	1665	1690
C=Cstr	1591.2	1593.1
C-Nstr	1315.4	1325
C-Hbend, C-Nbend	1247.9	1255.6
C-Hrock	651.9-744.5	663.5-750.9
C-Cstr	1110.9	1157.2
M-N	617.2	489.9

Conclusion

In this work, the structures, Frontier molecular orbitals, UV-visible and IR absorption spectra of the complexes $[Ni(L)_2]$ have been computed by means DFT and TD-DFT methods. Calculated structural parameters agree with experimental data, except for the Ni-N_1 and Ni-O_2 bond lengths, which are slightly longer than experimental values. HOMO and H-1 orbitals of the studied complex are mainly delocalized on the phenolate rings and on d-metal orbitals. The unoccupied orbitals LUMO and L+1 are overall delocalized on $\pi^*_{Phenolate}$ Computed energy gaps of the studied complex in the two solvents are almost equal, while calculated energy gaps with both functionals B3pw91 and Pbe0 are overall different. The simulated absorption spectra of complex $[Ni(L)_2]$ reproduce the main characteristics of the corresponding experimental spectra. The simulated absorption spectrum obtained with B3pw91 redshift the PBE0 one. The band observed in the visible region is assigned to S_0-S_7 absorption of mixed character LLCT/MLCT. The observed shoulder around ~298 nm is assigned to S_0-S_{11} absorption. The intense band observed around ~249 nm can be assigned to the occurred band in the PBE0 spectrum ~284 nm contributed by the transitions S_0-S_{24}, S_0-S_{33} and S_0-S_{34} which have mainly an LLCT character. Also we have been synthesized a Schiff base liagnd and two complexes Cu(II); Co5(II) and we characterized them using IR and NMR (^{1}H, ^{13}C).

Refrences

1- Alagona G, Ghio C, Rocchiccioli S (2007) Computational prediction of the regio- and diastereoselectivity in a rhodium-catalyzed hydroformylation/cyclization domino process. J Mol Model 13: 823–837. https://doi.org/10.1007/s00894-007-0205-8

2- Zhang T-T, Qi X-X, Jia J, Wu H-S (2012) Tuning electronic structure and photophysical properties of [Ir(ppy)2(py)2]+ by substituents binding in pyridyl ligand: a computational study. J Mol Model 18:4615–4624. https://doi.org/10.1007/s00894-012-1462-8

3- Chen M, Serna P, Lu J, Gates BC, Dixon DA (2015) Molecular models of site-isolated cobalt, rhodium, and iridium catalysts supported on zeolites: ligand bond dissociation energies. Comput Theor Chem 1074:58–72. https://doi.org/10.1016/j.comptc.2015.09.004

4- Meng Q, Shen W, Li M (2011) Mechanism of intermolecular hydroacylation of vinylsilanes catalyzed by a rhodium(I) olefin complex: a DFT study. J Mol Model 18:1229–1239. https://doi. org/10.1007/s00894-011-1151-z

5- Ahn SY, Ha Y (2009) The blue phosphorescent iridium complexes containing new triazole ligands for OLEDs. Mol Cryst Liq Cryst 504:59–66. https://doi.org/10.1080/15421400902939504

6- Park S-Y, Kim H-K, Shin D-M (2016) Synthesis and characterization of red phosphorescent iridium(III) complexes based on electron-acceptor modulation of main ligand for high efficiency organic light-emitting diodes. Mol Cryst Liq Cryst 636:38–44. https://doi.org/10.1080/15421406.2016.1200941

7- Simpson PV, Schmidt C, Ott I, Bruhn H, Schatzschneider U (2013) Synthesis, cellular uptake and biological activity against pathogenic microorganisms and cancer cells of rhodium and iridium Nheterocyclic carbene complexes bearing charged substituents. Eur J Inorg Chem 2013:5547–5554. https://doi.org/10.1002/ejic. 201300820

8- Almodares Z, Lucas SJ, Crossley BD, Basri AM, Pask CM, Hebden AJ, Phillips RM, McGowan PC (2014) Rhodium, iridium, and ruthenium half-sandwich picolinamide complexes as anticancer agents. Inorg Chem 53:727–736. https://doi.org/10.1021/ic401529u

9- Leung C-H, Zhong H-J, Chan DS-H, Ma D-L (2013) Bioactive iridium and rhodium complexes as therapeutic agents. Coord Chem Rev 257: 1764–1776. https://doi.org/10.1016/j.ccr.2013.01.034
10- Lan-Qin Chai, Gang Liu, Yu-Li Zhang, Jiao-Jiao Huang & Jun-Feng Tong (2013) Synthesis, crystal structure, fluorescence, electrochemical property, and SOD-like activity of an unexpected nickel(II) complex with a quinazoline-type ligand, Journal of Coordination Chemistry, 66:22, 3926-3938, DOI: 10.1080/00958972.2013.857016
11- Gary L. Miessler, St. Olaf College, Paul J. Fischer, Macalester College. Inorganic chemistry. — Fifth edition. Page 313.
12- Advanced Inorganic chemistry by F. Albert Cotton And Geoffrey Wilkinson F.R.S, P. 528,529.
13- Red Book p. 146
14- Cotton, Frank Albert; Geoffrey Wilkinson; Carlos A. Murillo (1999). Advanced Inorganic Chemistry. Wiley-Interscience. p. 1355.
15- Miessler, Gary L.; Paul J. Fischer; Donald Arthur Tarr (2013). Inorganic Chemistry. Prentice Hall. p. 696.
16- PAC, 1994, 66, 1077 (Glossary of terms used in physical organic chemistry (IUPAC Recommendations 1994)) on page 1100.
17- https://chem.libretexts.org/Bookshelves/General_Chemistry/Map%3A_General_Chemistry_(Petrucci_et_al.)/24%3A_Complex_Ions_and_Coordination_Compounds/24.01%3A_Werner%E2%80%99s_Theory_of_Coordination_Compounds
18- Inorganic_Chemistry_Atkins_Shriver P. 211
19- Enzyme Kinetics: Catalysis and Control: A Reference of Theory and Best-Practice Methods P.86
20- https://courses.lumenlearning.com/introchem/chapter/oxidation-numbers-of-metals-in-coordination-compounds/
21- Inorganic_Chemistry_Atkins_Shriver P.473
22- Ballhausen, Carl Johan,"Introduction to Ligand Field Theory",McGraw-Hill Book Co., New York, 1962
23- Griffith, J.S. (2009). The Theory of Transition-Metal Ions (re-issue ed.). Cambridge University Press.
24- Schläfer, H. L.; Gliemann, G. "Basic Principles of Ligand Field Theory" Wiley Interscience: New York; 1969

25- G. L. Miessler and D. A. Tarr “Inorganic Chemistry” 3rd Ed, Pearson/Prentice Hall publisher
26- Mulliken, Robert S. (July 1932). "Electronic Structures of Polyatomic Molecules and Valence. II. General Considerations".
27- 1930-2007., Cotton, F. Albert (Frank Albert), (1990). Chemical applications of group theory (3rd ed.). New York: Wiley. p. 102.
28- Albright, T. A.; Burdett, J. K.; Whangbo, M.-H. (2013). Orbital Interactions in Chemistry. Hoboken, N.J.: Wiley.
29- Coordination Chemistry, F.Basolo, R.C.Johnson, P. 37
30- https://chem.libretexts.org/Bookshelves/Organic_Chemistry/Supplemental_Modules_(Organic_Chemistry)/Fundamentals/Ionic_and_Covalent_Bonds.
31- Inorganic Chemistry Atkins.Shriver P 227 228 229 499 500
32- file:///F:/Article%20chimie%20project/transitions.pdf
33- Undergraduate Quantum Chemistry, Jussi Eloranta P 349
34- Inorganic Chemistry Atkins.Shriver P 497 498 499
35- L.A. Woodward, Introduction to the Theory of Molecular Vibration and Vibrational Spectroscopy, Oxford University Press, London, 1972
36- Inorganic Chemistry Atkins.Shriver P 231 232 233 235
37- Physical Chemistry Peter Atkins, Julio de Paula P 254 255 256
38- Introduction to Computational Chemistry,2 Edition, P 232 233 235 236
39- Undergraduate Quantum Chemistry, Jussi Eloranta.
40- C. A. Ullrich, Time-dependent density-functional theory: concepts and applications (Oxford University Press, 2012)
41- K. Harumiya, H. Kono, Y. Fujimura, I. Kawata, and A. D. Bandrauk, Phys. Rev. A 66, 043403 (2002)
42- N. Helbig, J. I. Fuks, M. Casula, M. J. Verstraete, M. A. L. Marques, I. V. Tokatly, and A. Rubio, Phys. Rev. A 83, 032503 (2011)
43- E. Runge and E. K. U. Gross, Phys. Rev. Lett. 52, 997 (1984).
44- E. Engel and R. M. Dreizler, Density functional theory: an advanced course (Springer, Berlin, 2012).
45- P. Hohenberg and W. Kohn, Phys. Rev. 136, B864 (1964)
46- W. Kohn and L. J. Sham, Phys. Rev. 140, A1133 (1965).

47- R. van Leeuwen, Phys. Rev. Lett. 80, 1280 (1998).

48- G. Vignale, Phys. Rev. A 77, 062511 (2008)

49- M. Lein and S. Kummel, Phys. Rev. Lett. ¨ 94, 143003 (2005).

50- Carsten A. Ullrich , Time-dependent density-functional theory: features and challenges, with a special view on matter under extreme conditions

51- W. Demtröder (2003). Laser Spectroscopy: Basic Concepts and Instrumentation

52- James W. Robinson (1996). Atomic Spectroscopy

53- Hilborn, Robert C. (1982). "Einstein coefficients, cross sections, f values, dipole moments, and all that"

54- Undergraduate Quantum Chemistry P 344 345

55- "Computational Chemistry Using the PC" ,Third Edition, Donald W. Rogers P 1516 17

56- R; Hehre, W.J; Pople, J. A. (1971). "Self-Consistent Molecular-Orbital Methods. IX. An Extended Gaussian-Type Basis for Molecular-Orbital Studies of Organic Molecules".J.Chem.Phys.**54**(2):724728.Bibcode:1971JChPh..54..724D. doi:10.1063/1.1674902

57- Moran, Damian; Simmonett, Andrew C.; Leach, Franklin E. III; Allen, Wesley D.; Schleyer, Paul v. R.; Schaefer, Henry F. (2006). "Popular theoretical methods predict benzene and arenes to be nonplanar". J. Am. Chem. Soc. 128 (29): 9342–9343. doi:10.1021/ja0630285

58- Dunning, Thomas H. (1989). "Gaussian basis sets for use in correlated molecular calculations. I. The atoms boron through neon and hydrogen". J. Chem. Phys. 90 (2): 1007–1023. Bibcode:1989JChPh..90.1007D. doi:10.1063/1.456153

59- Pye CC, Xidos JD, Poirer RA, Burnell DJ (1997) J Phys Chem A 101:3371, Rudolph W, Brooker MH, Pye CC (1995) J Phys Chem 99:3793

60- Gourbatsis, S., et al., *The coordination chemistry ofN, N'-ethylenebis (2-acetylpyridine imine) andN, N'-ethylenebis (2-benzoylpyridine imine); two potentially tetradentate ligands containing four nitrogen atoms.* Transition Metal Chemistry, 1990. **15**(4): p. 300-308.

Abstract

In this work, the structures, Frontier molecular orbitals, UV-visible and IR absorption spectra of the complexes $[Ni(L)_2]$ have been computed by means DFT and TD-DFT methods. Also we have been synthesized a Schiff base ligand and two complexes Cu(II); Co(II) and we characterized them using IR and NMR (^1H, ^{13}C).

Key words: Ligands, Nickel (II), Cobalt (II), Copper (II), Metal complex, Infrared, Uv-visible, DFT, TDDFT, NMR.

Résumé

Dans ce travail, les structures, les orbitales moléculaires frontier, les spectres d'absorption UV-visible et IR des complexes $[Ni(L)_2]$ ont été calculées à l'aide des méthodes DFT et TD-DFT. Nous avons aussi synthétisé un ligand d'une base de Schiff et deux complexes Cu (II); Co(II) et nous les avons caractérisées par IR et RMN (^1H, ^{13}C).

Mots clés: Ligands, Nickel (II), Cobalt (II), Copper (II), complexe, Infrarouge, Uv-visible, DFT, TDDFT, RMN.

ملخص

في هذا العمل، قمنا بدراسة بنية المعقد السابق، المدارات الجزيئية الحدودية وأطياف الامتصاص البنفسجية-المرئية وتحت الحمراء للمعقد $[Ni(L)_2]$ باستعمال النظرية الوظيفية للكثافة والنظرية الوظيفية للكثافة المتعلقة بالزمن. كذلك قمنا بتصنيع رُبيطة Schiff base ومعقدين Cu(II) و Co(II) وقمنا بتحليلهما بواسطة IR و NMR (^1H, ^{13}C).

الكلمات المفتاحية

Ligands, Nickel (II), Cobalt (II), Copper (II), Metal complex, Infrared, Uv-visible, DFT, TDDFT, NMR.